Journal of Asian Earth Sciences 63 (2013) 179–196

Contents lists available at SciVerse ScienceDirect

Journal of Asian Earth Sciences

journal homepage: www.elsevier.com/locate/jseaes

Ion microprobe U–Th–Pb geochronology and study of micro-inclusions in zircon from the Himalayan high- and ultrahigh-pressure eclogites, Kaghan Valley of Pakistan

Hafiz Ur Rehman [a,*], Katsura Kobayash [b], Tatsuki Tsujimori [b], Tsutomu Ota [b], Hiroshi Yamamoto [a], Eizo Nakamura [b], Yoshiyuki Kaneko [c], Tahseenullah Khan [d], Masaru Terabayashi [e], Kenta Yoshida [f], Takao Hirajima [f]

[a] Graduate School of Science and Engineering, Kagoshima University, Korimoto 1-21-35, Kagoshima 890-0065, Japan
[b] The Pheasant Memorial Laboratory, Institute for Study of the Earth's Interior, Okayama University, Misasa, Tottori 682-0193, Japan
[c] Department of Education, Meisei University, 2-1-1 Hodokubo, Hino-shi, Tokyo 191-8506, Japan
[d] Department of Earth and Environmental Sciences, Bahria University, Shangrila Road, Sector E-8, Islamabad, Pakistan
[e] Department of Safety Systems Construction Engineering, Kagawa University, Takamatsu, Kagawa 761-0396, Japan
[f] Department of Geology and Mineralogy, Kyoto University, Kyoto 606-8502, Japan

ARTICLE INFO

Article history:
Received 13 January 2012
Received in revised form 4 April 2012
Accepted 30 April 2012
Available online 9 May 2012

Keywords:
U–Th–Pb geochronology
HR-SIMS
Zircon internal structures
Micro-inclusions
Himalayan UHP eclogites
Kaghan Valley

ABSTRACT

We report ion microprobe U–Th–Pb geochronology of in situ zircon from the Himalayan high- and ultrahigh-pressure eclogites, Kaghan Valley of Pakistan. Combined with the textural features, mineral inclusions, cathodoluminescence image information and the U–Th–Pb isotope geochronology, two types of zircons were recognized in Group I and II eclogites. Zircons in Group I eclogites are of considerably large size (>100 μm up to 500 μm). A few grains are euhedral and prismatic, show oscillatory zoning with distinct core–rim luminescence pattern. Several other grains show irregular morphology, mitamictization, embayment and boundary truncations. They contain micro-inclusions such as muscovite, biotite, quartz and albite. Core or middle portions of zircons from Group I eclogites yielded concordant U–Th–Pb age of 267.6 ± 2.4 Ma (MSWD = 8.5), have higher U and Th contents with a Th/U ratio > 1, indicating typical magmatic core domains. Middle and rim or outer portions of these zircons contain inclusions of garnet, omphacite, phengite and these portions show no clear zonation. They yielded discordant values ranging between 210 and 71 Ma, indicating several thermal or Pb-loss events during their growth and recrystallization prior to or during the Himalayan eclogite-facies metamorphism. Zircons in Group II eclogites are smaller in size, prismatic to oval, display patchy or sector zoning and contain abundant inclusions of garnet, omphacite, phengite, quartz, rutile and carbonates. They yielded concordant U–Th–Pb age of 44.9 ± 1.2 Ma (MSWD = 4.9). The lower U and Th contents and a lower Th/U ratio (<0.05) in these zircons suggest their formation from the recrystallization of the older zircons during the Himalayan high and ultrahigh-pressure eclogite-facies metamorphism.

1. Introduction

Generally, dating of the eclogite-facies rocks is a difficult task because low metamorphic temperatures, incomplete mineral recrystallization, retrograde overprinting, excess-Ar and Pb-loss, all hamper the use of thermo chronometers such as Rb–Sr, Ar–Ar, or Sm–Nd (e.g., Arnaud and Kelley, 1995). Zircon, the most resistant mineral to alteration after diamond, its retaining information of growth and recrystallization, its relative chemical inertness, high retentivity for radiogenic Pb, and strong preference for U over Pb during crystallization (Wasserburg et al., 1969; Krogh, 1973; Compston et al., 1984; Parrish and Krogh, 1987; Ashwal et al., 1999), is widely used for determination of thermal history of igneous, and metamorphic rocks (e.g., Belousova et al., 2002; Rubatto and Hermann, 2003). Particularly, the ion microprobe U–Th–Pb age-dating has been successful in several high temperature, high- and ultrahigh-pressure (UHP) terrains (e.g., Gebauer, 1996; Rubatto et al., 1998, 1999; Liati and Gebauer, 1999; Hermann et al., 2001; Liu et al., 2006; Parrish et al., 2006; Zheng et al., 2006). However, in mafic rocks zircons are less common and smaller in size and they contain lower amounts of U, Th, Pb compared to those in felsic rocks. The chemical and physical heterogeneity in single zircon crystals in mafic rocks make them difficult for geologically

* Corresponding author. Tel.: +81 99 285 8147; fax: +81 99 259 4720.
E-mail address: hafiz@sci.kagoshima-u.ac.jp (H.U. Rehman).

1367-9120/$ - see front matter © 2012 Elsevier Ltd. All rights reserved.
http://dx.doi.org/10.1016/j.jseaes.2012.04.025

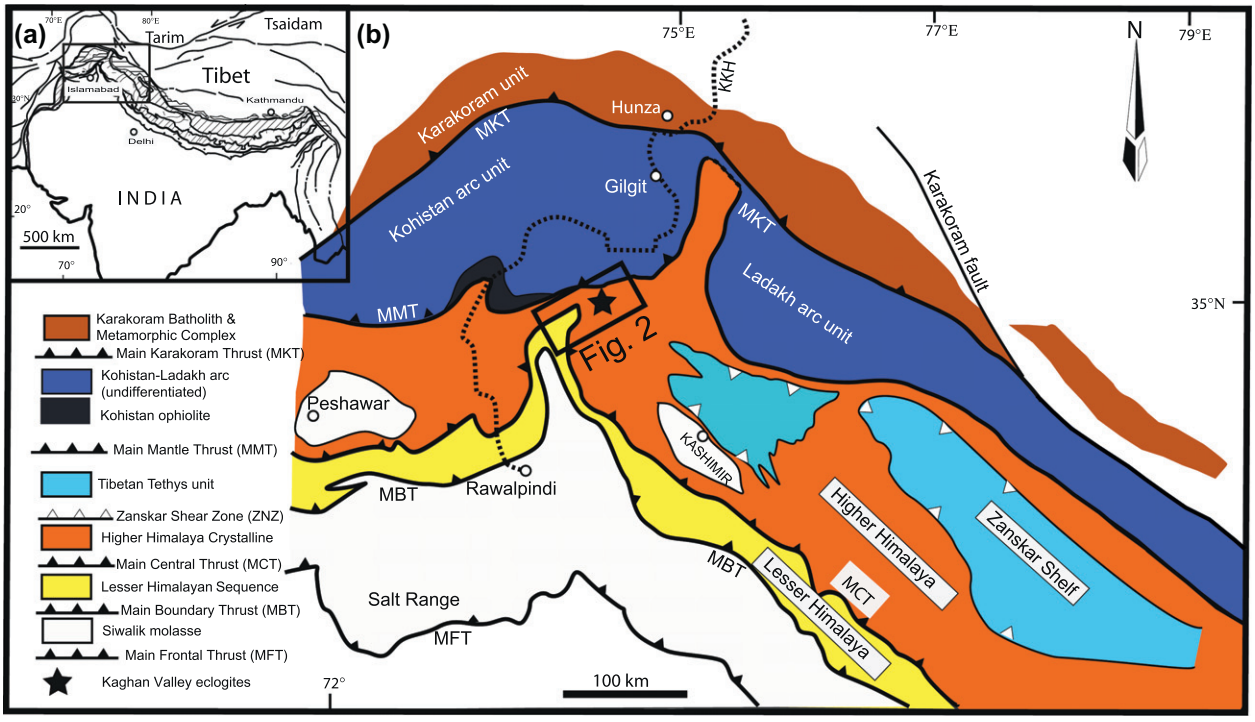

Fig. 1. (a) Tectonostratigraphic map and geographical location of the Himalayan mountain range. Portion enclosed in a rectangle is the enlarged map shown in (b). (b) Geological map of the Western part of Himalaya showing major tectonic blocks i.e. the Indian Plate, the Kohistan-Ladakh arc, and the Asian Plate. Filled star and a rectangle surrounding it represent location of the Kaghan Valley.

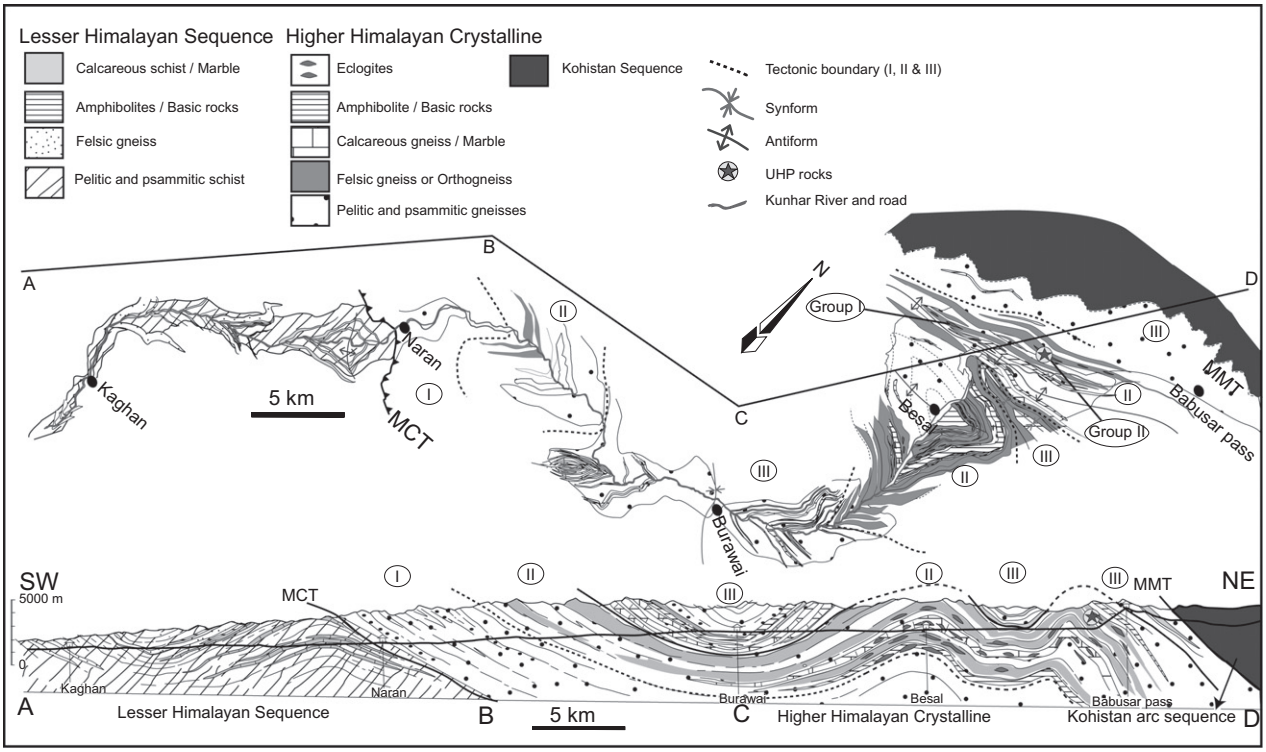

Fig. 2. Geological map and a cross-section of the Himalayan Metamorphic Belt along the Kaghan Valley Transect (modified after Kaneko et al., 2003; Rehman et al., 2007). Locations of Group I and II eclogites are marked.

meaningful age-dating. Several questions need to be clarified before interpreting the geochronological results from such types of zircons for example: (1) whether the internal structure of individual zircon grains is known even if they are small? (2) What are the

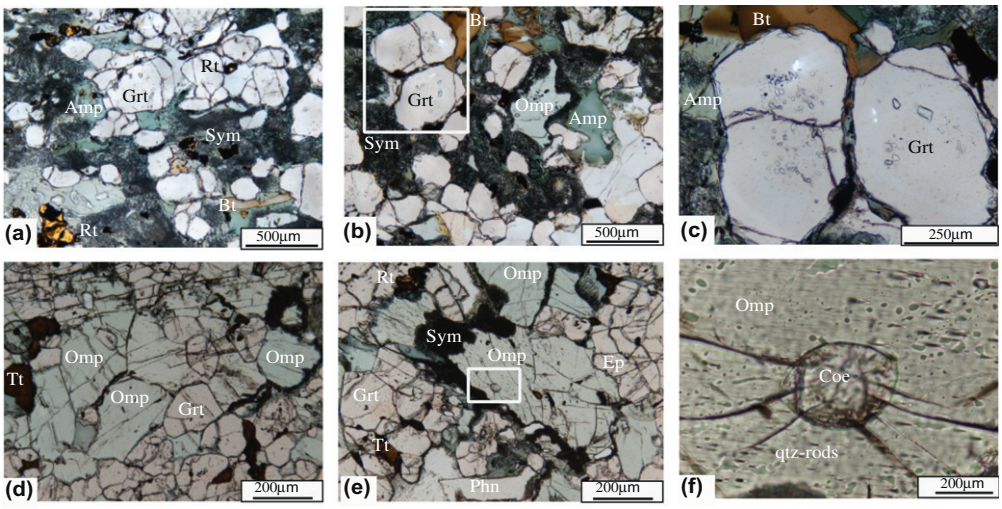

Fig. 3. Photomicrographs of Group I and II eclogites showing typical textures of eclogite-facies grade. Photomicrographs (a–c) show Group I eclogites containing abundant rutile and titanite. Most of the clinopyroxene is retrogressed to amphibole and quartz–albite–jadeite symplectites. (b) Amphibole and biotite developed during retrogressive stage. (c) Enlarged portion of white rectangle on photomicrograph "b" shows retrogressed omphacite and partly retrogressed (rim parts) garnet. Garnet contains inclusions of quartz + omphacite ± epidote ± zircon. (d) Photomicrograph of Group II eclogites in which omphacite still remains with less retrogressed part. Garnet is also fresh and unaltered. (e) Group II eclogites with typical UHP metamorphic grade mineral (e.g., coesite relics in omphacite). (f) An enlarged portion of the white rectangle in photomicrograph "e" in which coesite relics with palisade texture and radial cracks are visible. Note the presence of quartz rods and exsolution lamellae in the same grain of omphacite. Abbreviations: Amp, amphibole, Bt, biotite; Coe, coesite; Ep: epidote; Grt, garnet; Omp, omphacite; Sym, symplectites; Rt, rutile; and Tt, titanite.

chemically different compositional domains within a single zircon grain? And (3) what kinds of micro-inclusions are there in the compositionally distinct domains?

In the present research we tried to elucidate the protolith-related information preserved in igneous zircons preserved within the HP and UHP eclogites of the Kaghan Valley, Pakistan Himalaya and to understand the complex history of metamorphic evolution in the compositionally distinct domains of metamorphic zircons within these rocks. For this purpose, we studied zircon internal structures, zoning patterns via cathodoluminescence (CL) imaging assisted by micro-inclusion assemblage via micro-Raman spectroscopy in various domains of zircon grains. Our results led us to extrapolate geochronological and metamorphic records the Himalayan eclogites have experienced from their emplacement till their exhumation.

2. Geological setting

In the northwestern part of Pakistan, rocks of the Indian and Asian plates, sandwiching an intra-oceanic Kohistan-Ladakh island arc (KLA), represent a classical example of continent–continent collision and subduction tectonics (Fig. 1). The KLA is separated in the south from the Indian plate by ophiolitic mélange and a suture zone termed as the Indus Suture or the Main Mantle Thrust (MMT) and in the north from the Asian Plate by another suture termed as the Shyok Suture or the Main Karakoram Thrust (MKT) (Tahirkheli, 1979; Beck et al., 1995; Searle et al., 1999; Rehman et al., 2011 and references therein). Lithological details of the KLA and Asian Plate are not presented here because they are out of the scope of this paper. In the following sections we focus mainly on the rocks of Indian Plate.

In the Kaghan Valley a thick sequence of Proterozoic to Paleogene rocks of the Indian Plate, metamorphosed to various grades, are exposed south of the MMT (Fig. 2). The grade of metamorphism increases from low-grade greenschist-facies in the south to HP and UHP eclogite-facies grade in the north (Greco et al., 1989; Treloar et al., 1989, 2003; Pognante and Spencer, 1991; O'Brien et al., 2001; Kaneko et al., 2003; Rehman et al., 2007). To the south lie strongly folded and sheared rocks of the Precambrian to Eocene age (Honegger et al., 1982) comprising the Lesser Himalayan Sequence (LHS). These metamorphic rocks are of chlorite- to biotite- to garnet-grade in the south and reach up to staurolite-grade in the north (Rehman et al., 2007) near the Main Central Thrust (MCT; a north-dipping reverse fault carrying the LHS schists and gneisses on its hanging wall) (Greco et al., 1989). The most abundant lithologies in the LHS are fine-grained pelitic and psammitic schists with sporadic marble bands and mafic rock layers of greenschist-facies. To the north of the LHS lies the Higher Himalayan Crystalline (HHC) sequence separated from the former by the MCT. The HHC is comprised of the basement (Unit I), middle or lower cover (Unit II) and upper cover (Unit III) (Greco et al., 1989; Kaneko et al., 2003; Rehman et al., 2007). Unit I is composed of psammitic, pelitic and calcareous rocks intruded by deformed basic dikes and sills. Unit II, representing the major UHP unit, is comprised of coarse-grained garnetiferrous felsic gneisses, marbles, and amphibolites with locally abundant eclogites. Eclogites are exposed as small lenticular bodies interlayered with felsic gneisses of the UHP grade (Kaneko et al., 2003) and marbles. Unit III, the top most tectonic unit of the HHC, is comprised of siliceous schists, pelitic/psammitic gneisses, marbles, amphibolites and amphibolitized eclogites overlain by the Kohistan-Ladakh arc sequence (Rehman et al., 2007). Pressure–temperature (P–T) estimates and a comprehensive thermobaric structure of the Himalayan metamorphic belt along the Kaghan Valley transect have been presented elsewhere (see Rehman et al., 2007).

The Himalayan eclogites in the Kaghan Valley were formed by the subduction of the Indian Plate slab beneath the Asian Plate after the India–Asia collision in the Eocene and experienced UHP event (Tonarini et al., 1993; Spencer et al., 1995; Kaneko et al., 2003; Parrish et al., 2006; Rehman et al., 2007, 2008; Wilke et al., 2010a,b). Protolith rocks of these eclogites were considered as the Permian Panjal Trap basalts (Honegger et al., 1982). Rehman et al. (2008) classified the Himalayan eclogites exposed in the Kaghan Valley into two groups based on field occurrence, petrography and major and trace element geochemistry. Group I eclogites which are intercalated with pelitic gneisses and marbles are massive and range in size from a few meters to few tens of meters in

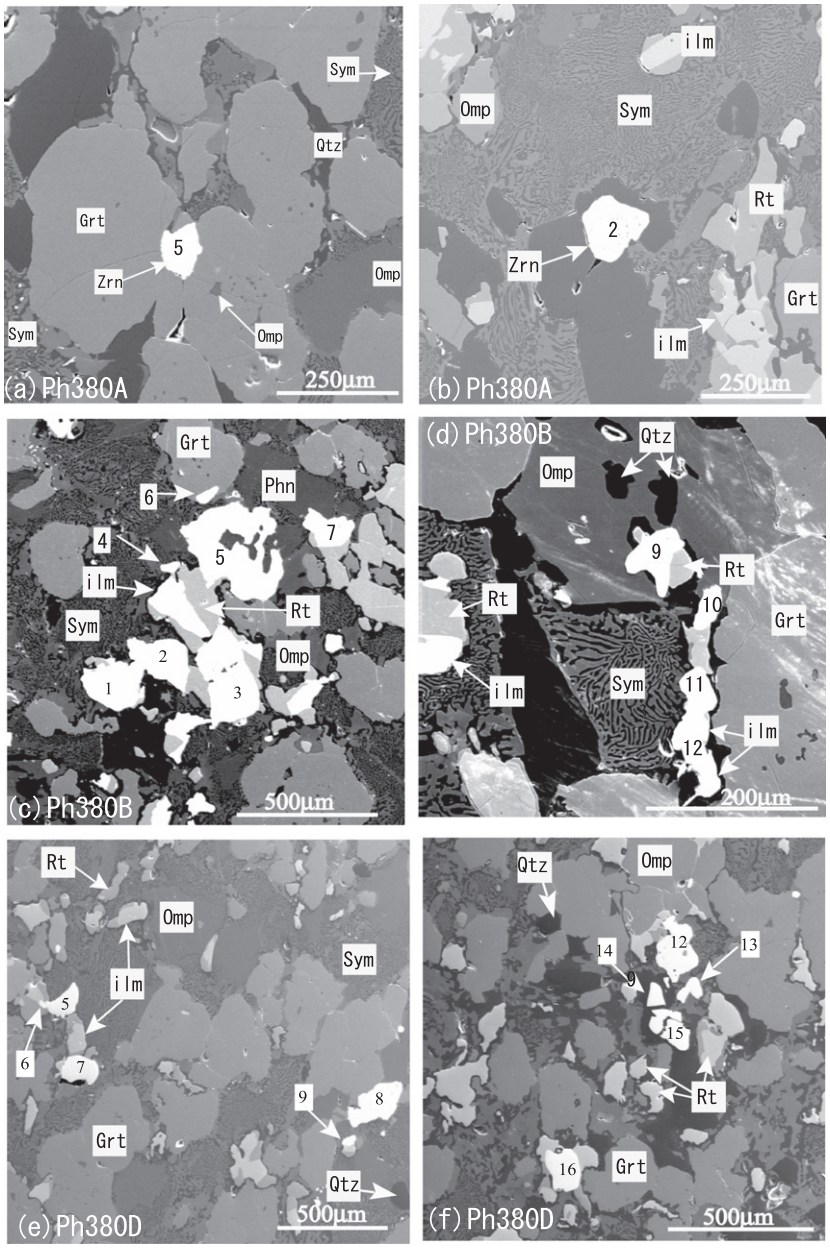

Fig. 4. Scanning electron microscope (SEM) images of Group I eclogites. Textural features indicate eclogites-facies mineral assemblage, retrogressed phase in the form of quartz–albite–amphibole symplectites and abundantly occurring zircons in the Group I eclogites. (a) SEM image illustrating zircon euhedral grain developed along the grain boundaries of clustered garnet. (b) SEM image of the Group I eclogite displaying a zircon grain (>150 µm) included in quartz and surrounded by symplectites. In this portion of the thin section omphacite is retrogressed to symplectites. Figure (c) and (d) are portions of thin section displaying unusually abundant zircon grains of irregular shape. Figure (e) and (f) represent SEM images displaying zircon occurrence and textural relationships within the eclogite-facies assemblage. Digits on zircon grains show zircon label. Mineral abbreviations are same as explained in Fig. 3.

thickness and extend to a few hundred meters in length. They are coarse-grained, Fe–Ti rich (FeO: 15–18 wt.%, and TiO_2: 2–5 wt.%) and contain abundant zircons. These eclogites are composed of garnet + omphacite + quartz + rutile + titanite + amphibole + apatite + epidote/allanite + symplectite ± with accessory ilmenite preserving no UHP imprints (Fig. 3a–c). They record P–T conditions at 2.2 ± 0.3 GPa and 704 ± 92 °C (Rehman et al., 2012). At places these eclogites are strongly amphibolitized and contain abundant quartz–albite–amphibole symplectites (Fig. 3b).

Group II eclogites appear in thin layers which range from a few centimeters to two meters in width. These eclogites are fine- to medium-grained; comparatively less enriched in FeO and TiO_2 contents and contain a few zircons. They are composed of garnet + omphacite + phengite + quartz/coesite + titanite + amphibole + epidote + symplectite with accessory rutile, ilmenite, apatite and zircon (Fig. 3d–f). They are relatively fresh in which omphacite remains unchanged at the core or middle portions whereas rim portions are retrogressed to quartz–albite–amphibole symplectites (Fig. 3e). At places omphacite contains relics of coesite with typical palisade texture and radial cracks (Fig. 3f). In the same omphacite grain quartz rods and exsolution lamellae are observed (Fig. 3f). Peak P–T estimates in Group II eclogites show a range of 2.7–3.2 GPa and 757–786 °C indicating UHP conditions (Kaneko et al., 2003; Rehman et al., 2007). Coesite inclusions in clinopyroxene from eclogites (O'Brien et al., 2001; Rehman et al., 2007; Wilke et al., 2010a) and in zircon from felsic gneisses (Kaneko et al., 2003)

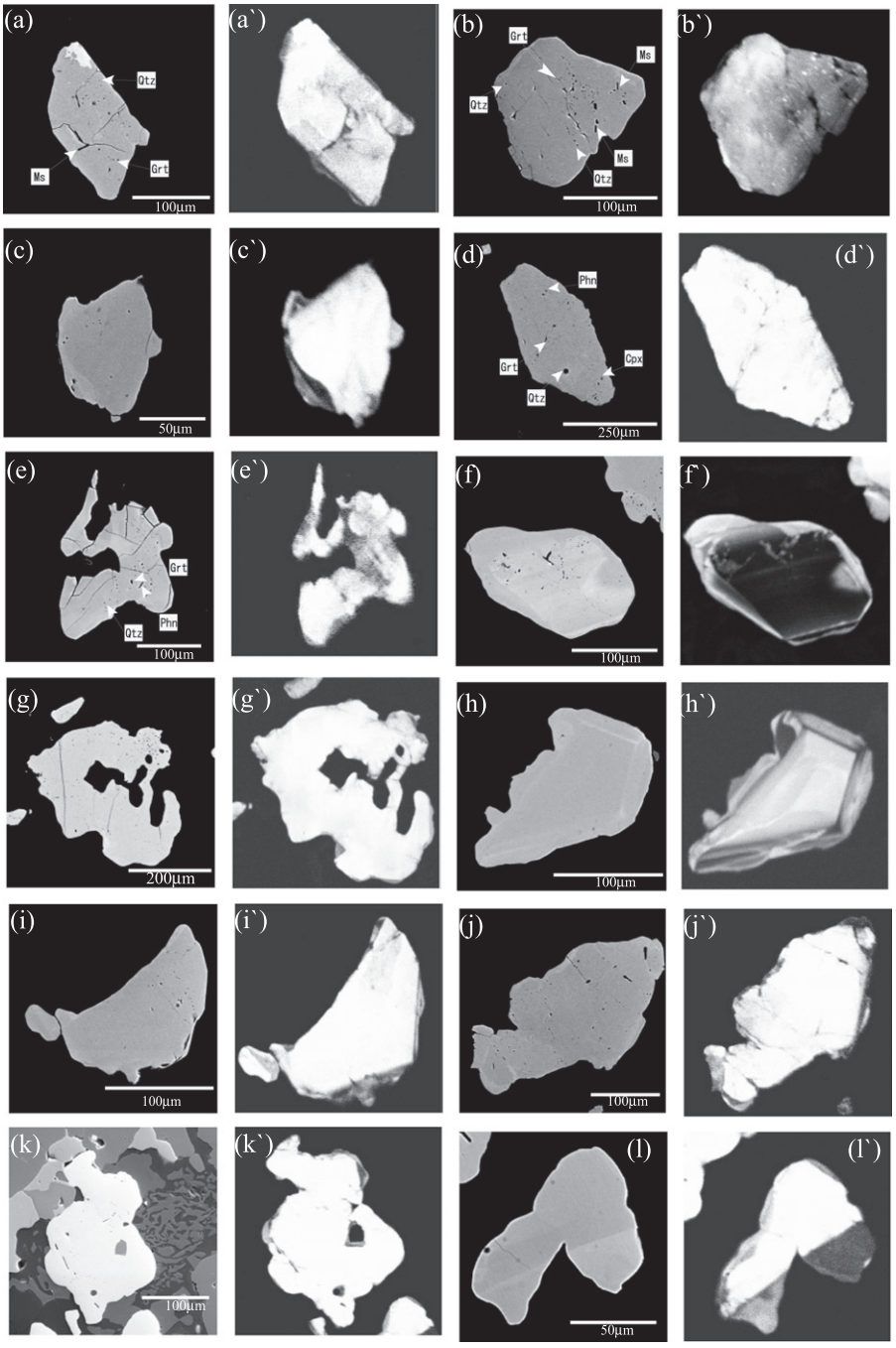

Fig. 5. Back-Scattered electron (BSE) (in the left with alphabets a–l) and CL (in the right with dashed alphabets a′–l′) images of zircons in Group I eclogites. Most of the zircons show no distinct zonation except thin CL-dark rims. Two euhederal zircon grains (f′ and h′) have typical magmatic zoning (Pidgeon, 1992).

confirm that these rocks subducted to depths >90 km and underwent UHP metamorphism.

3. Analytical procedure

Major part of the analytical work was conducted at the Pheasant Memorial Laboratory (PML), Institute for the Study of the Earth's Interior (ISEI), Okayama University, Misasa, Japan. Three circular thin sections (2.5 cm in diameter) from Group I eclogites which contained abundant zircons of considerable size (>100 µm) were selected for U–Th–Pb geochronology. Selected samples were polished with a paste of diamond (3 µm) and Al (1 µm). The samples were then chemically washed with HCl and HNO_3 to remove any surface contamination and common Pb. Polished thin sections were then studied under the scanning electron microscope (SEM) attached with an EDX-detector. Accelerating voltage of the SEM was 20 kV with a filament current of 3 nA and working distance was kept between 15 and 18 mm. For high-precision positioning of the identified grains, a Visual Stage System was used through a linkage with microscope, SEM-EDX, and the Secondary Ionization Mass Spectrometers (SIMSs). Three samples from Group II eclogites were crushed using a jaw crusher, and zircons were separated from the crushed fraction using isodynamic and heavy liquid separation methods. Finally, zircon grains were hand-picked under optical microscope. Separated grains were mounted in epoxy resin, polished in the same way as

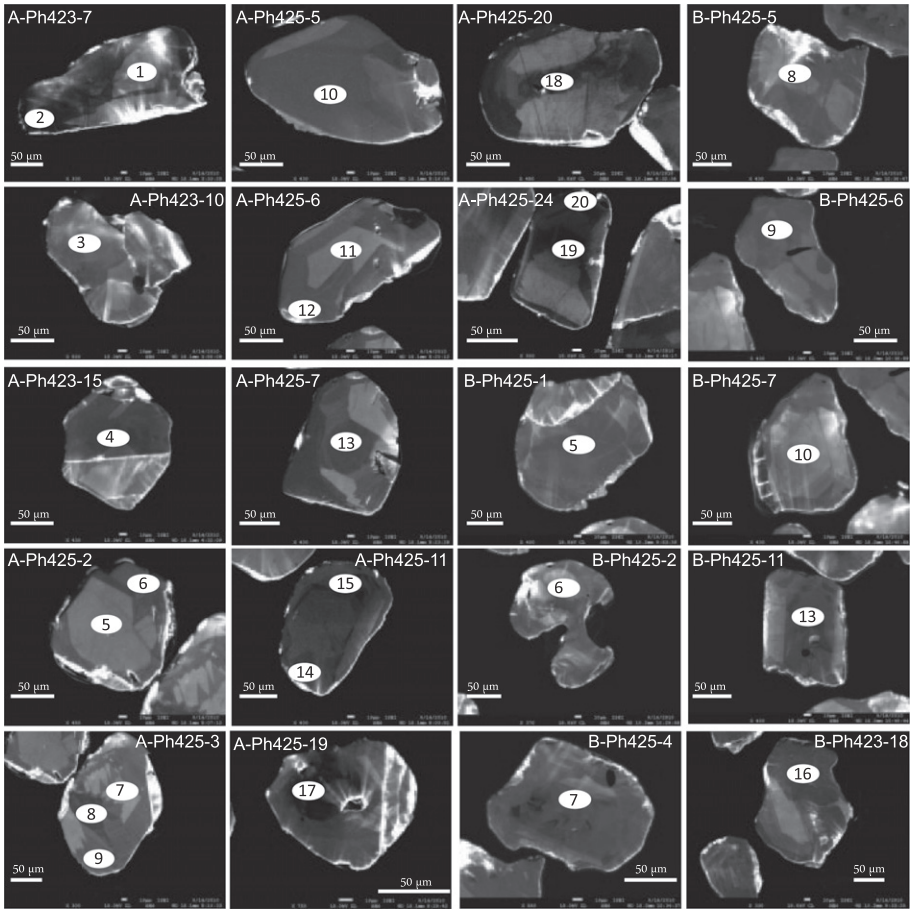

Fig. 6. CL images of Group II eclogites with sector or patchy zoning, typical for metamorphic zircons (Hoskin and Black, 2000; Rubatto et al., 1999; Zheng et al., 2006). Numbered ellipses on zircons indicate the HR-SIMS Cameca-ims 1270 measurement spots. Zircon grains are labeled such as A-Ph423-7 and B-Ph425-11, where ''A and B'' represent discs on which zircons were mounted, followed by Ph (422, 423 and 425) which indicate sample numbers, and the digits after hyphen mark (-) represent label of the individual zircon grains. Same numbering system is used in Table 4.

explained above and were studied under the SEM. All the zircon grains from both groups of eclogites were photographed as SEM, back scattered electron (BSE), and CL images. Mineral phases trapped as micro-inclusions in the zircons were identified using SEM-EDX detector and micro-Raman spectroscopy. Inclusions exposed at the zircon surface were analyzed for their chemical composition with SEM-EDX detector, whereas those situated at the interiors were analyzed with micro-Raman spectrometers at Kyoto and Kagawa Universities. For comparison of chemical compositions of the inclusions with eclogite-facies minerals we analyzed matrix minerals particularly garnet and omphacite using electron probe micro analyzer situated at the ISEI.

A dynamic multi-collection method using High Resolution Secondary Ionization Mass Spectrometer (HR-SIMS Cameca-ims 1270) housed at the ISEI was applied for zircon age-dating. The in situ zircon grains were sputtered by an O^- primary beam with 15–30 nA intensity and −13.0 kV acceleration resulting in a beam size of 10–20 μm in diameter. The HR-SIMS at PML was equipped with four moveable secondary electron multipliers and a fixed one. The significance of this set up cancels the time drift of secondary ion beam intensity caused by the instability of primary ion beam and charging effect on the sample as well as the time reduction on data acquisition. In this system, four Pb isotopes (204, 206, 207 and 208) signals were detected simultaneously by individual multiplier appropriately configured on the focal plane. In a single run of one analysis after four Pb isotopes it detected signals from UO^+ by the movable center multiplier. Counting time for Pb^+ and UO^+ was 20 and 2 s respectively with waiting time of 0.5 s. In total 55 cycles were obtained in one run, taking approximately 25 min and about 10–13 min of pre-sputtering zircon surface, tuning secondary ion intensity maximum and mass calibration. Instrumental mass discrimination and mass fractionation for U–Pb isotopic ratios were obtained using the zircon standards (Sri Lanka zircon and 91500). Age calculations (U–Pb Concordia diagrams) were made using Isoplot/Ex version 3.6 (Ludwig, 2009).

4. Results

In total 52 zircon grains within three thin sections of Group I and 114 zircon grains from two circular mounts of Group II eclogites were studied. All the grains were studied for textural features under the polarizing microscope and a scanning electron microscope. Micro-inclusions in them were studied via SEM-EDX detector and micro-Raman spectrometer. Internal structures and zoning pattern were observed via CL imaging attached with the SEM. Details of the textural features, CL images, micro-inclusions and their chemical compositions are presented in the forthcoming sections.

4.1. Zircon occurrence, textural features, and internal structures

Zircons from both groups of eclogites have different morphologies, such as prismatic, isometric, oval and rounded (Figs. 4 and 5). They occur along grain boundaries (Fig. 4a) in most cases, however

Table 1
Mineral inclusions in zircon from Group I (HP) and Group II (UHP) eclogites of the Kaghan Valley, Pakistan Himalaya.

Group	Sample no.	Zircon grain no.	Inclusion type																		
			Coe	Qtz	Grt	Omp	Aug	Dio	Bt	Phe	Ms	Phl	Rt	Z	Ky	Sil	Cal	Dol	Ap	Gr	Mel	Hau
Group I	Ph380A	Zrn 2		+					+	+					+							
		Zrn 3		+	+	+			+	+			+		+							
		Zrn 4		+																		
		Zrn 5		+																		
		Zrn 6		+		+			+	+					+					+		
		Zrn 7		+		+				+					+							
		Zrn 9		+						+					+							
		Zrn 10		+											+							
		Zrn 13		+						+					+							
		Zrn 14		+	+	+				+					+							
		Zrn 15		+	+	+				+					+							
		Zrn 17		+						+					+							
		Zrn 18		+						+					+							
	Ph380B	Zrn 1		+		+									+							
		Zrn 2		+									+		+							
		Zrn 3		+		+				+					+							
		Zrn 4		+											+							
		Zrn 5		+						+					+							
		Zrn 6		+						+					+							
		Zrn 7		+											+							
		Zrn 9		+									+		+							
		Zrn 10		+																		
		Zrn 11		+						+					+							
		Zrn 13		+	+					+					+							
	Ph380D	Zrn 1		+						+												
		Zrn 2		+																		
		Zrn 4		+																		
		Zrn 5		+																		
		Zrn 7		+																		
		Zrn 8		+	+					+												
		Zrn 12		+	+					+												
		Zrn 13		+																		
		Zrn 14		+																		
		Zrn 15		+																		
		Zrn 17		+	+					+			+		+							
		Zrn 18		+						+			+		+							
		Zrn 19		+																		
Group II	Ph422A	Zrn 1		+		+			+		+	+	+									
		Zrn 2		+									+		+							
	Ph423A	Zrn 2		+	+	+				+			+		+							
		Zrn 4		+	+alm								+							+		
		Zrn 6		+		+				+			+									
		Zrn 7			+																	
		Zrn 13											+									
		Zrn 14			+	+				+			+								+	
		Zrn 15																				
		Zrn 16			+								+								+	
		Zrn 17																				
		Zrn 18				+	+															
		Zrn 19				+	+														+	+
		Zrn 20			+	+		+														+
		Zrn 21		+		+	+				+											
		Zrn 22			+																	
	Ph425A	Zrn 1				+							+									
		Zrn 2																				
		Zrn 3											+			+					+	+
		Zrn 4		+												+		+			+	

(*continued on next page*)

Table 1 (*continued*)

Group	Sample no.	Zircon grain no.	Inclusion type																		
			Coe	Qtz	Grt	Omp	Aug	Dio	Bt	Phe	Ms	Phl	Rt	Z	Ky	Sil	Cal	Dol	Ap	Gr	Mel	Hau
		Zrn 5																				
		Zrn 6																				
		Zrn 7																				
		Zrn 8																				
		Zrn 9		+		+							+					+				
		Zrn 10																				
		Zrn 11		+	+	+															+	+
		Zrn 12																				
		Zrn 13											+									
		Zrn 14											+									
		Zrn 15																				
		Zrn 16											+									
		Zrn 17											+					+				
		Zrn 18																				
		Zrn 19		+	+	+																
		Zrn 20																				
		Zrn 21																				
		Zrn 22																				
		Zrn 23																				
		Zrn 24			+																	
		Zrn 25																				
		Zrn 26			+								+									
	PH422B	Zrn 1		+	+	+				+			+		+							
		Zrn 2																				
		Zrn 5																				
		Zrn 6																				
		Zrn 7		+																		
	PH423B	Zrn 1		+																		
		Zrn 2		+																		
		Zrn 3		+	+					+												
		Zrn 4											+									
		Zrn 5																				
		Zrn 6																				
		Zrn 7																				
		Zrn 8																				
		Zrn 9																				
		Zrn 10																				
		Zrn 11				+							+									
		Zrn 13																				
		Zrn 14											+									
		Zrn 15											+									
		Zrn 16								+												
		Zrn 17			+																	
		Zrn 18																				
		Zrn 19			+								+									
		Zrn 20																				
		Zrn 21											+									
		Zrn 22																				
		Zrn 23																				
	PH425B	Zrn 1																				
		Zrn 2											+									
		Zrn 3																				
		Zrn 4				+																
		Zrn 5																				
		Zrn 6			+																	
		Zrn 7																				
		Zrn 8																				
		Zrn 9																				
		Zrn 10																				
		Zrn 11											+									
		Zrn 12																				
		Zrn 13																				
		Zrn 14																				
		Zrn 15																				
		Zrn 16											+									
		Zrn 17																				
		Zrn 18																				
		Zrn 19																				
		Zrn 20																				

Table 1 (*continued*)

Group	Sample no.	Zircon grain no.	Inclusion type																			
			Coe	Qtz	Grt	Omp	Aug	Dio	Bt	Phe	Ms	Phl	Rt	Z	Ky	Sil	Cal	Dol	Ap	Gr	Mel	Hau
		Zrn 21																				
		Zrn 22			+	+																
		Zrn 23																				
		Zrn 24																				
		Zrn 25																				
		Zrn 26											+									
		Zrn 27			+																	
		Zrn 28																				
		Zrn 29																				
		Zrn 30																				
		Zrn 31				+																

Mineral abbreviations used: Coe: coesite, Qtz: quartz, Grt: garnet, Omp: omphacite, Aug: augite, Dio: diopsite, Phe: phengite, Ms: muscovite, Bt: biotite, Phl: phlogopite, Rt: rutile, Zs: zoicite, Ky: kyanite, Sil: sillimanite, Dol: dolomite, Cal: calcite, Ap: apatite, Gr: graphite, Mel: melelite, Hau: hauyne. Alm marked inside the table means almandine.

in some cases they also occur as inclusions (Fig. 4b). In Group I eclogites, at places, they form clusters (e.g., sample Ph380B, Ph380D) (Fig. 4c). Several zircon grains are closely associated with rutile and ilmenite (Fig. 4d). Most of the zircons in Group I eclogites are colorless to light pink, transparent. Maximum grains are subhederal to euhederal and prismatic whereas several grains are irregular in shape with common embayment (Zrn 5 in Fig. 4c). Back-scattered and CL images show that most of the zircon grains in Group I eclogites are not zoned or show tiny CL-dark rims, with no obvious core–rim structure (Fig. 5) except two prismatic grains (Fig. 5f and h) which have microscopically visible cores. They display oscillatory zoning with CL-broad cores and CL-thin rims. A few other grains show patchy zoning with cloudy thin rims.

Zircons in Group II eclogites are smaller in size (10–200 μm). They are prismatic, short, subhederal to euhederal. The CL images show sector or patchy zoning with no regular pattern (Fig. 6).

4.2. Micro-inclusion assemblage in zircon and their chemical composition

Various mineral phases were identified as inclusions at the surface and within the zircon grains with SEM-EDX detector and micro-Raman spectroscopy. Types of inclusions in individual zircon grains from Group I and II eclogites are shown in Table 1. Zircons in Group I eclogites contain inclusions of low-P minerals such as quartz, plagioclase, muscovite, biotite and carbonates in the core or middle portions indicating pre-eclogite-facies stage. A few grains also contain inclusions of omphacite, garnet, phengite and rutile, indicating that these zircons were formed during eclogite-facies stage. Chemical composition of the primary and/or peak metamorphic stage minerals such as omphacite and garnet in Group I eclogites are more or less obliterated during pervasive retrograde metamorphism. Therefore no UHP minerals were recorded in the Group I eclogites. In the matrix assemblage of Group I eclogites omphacite and phengite are replaced by the amphibolite-facies assemblage such as amphibole, biotite and quartz–albite–jadeite symplectites. Titanite has also been developed ubiquitously as a secondary mineral after the replacement of rutile and probably Ca-component of clinopyroxene. Micro-inclusions in zircon such as omphacite, garnet, phengite and quartz were compositionally distinct from the matrix assemblage (Tables 2 and 3).

Micro-inclusions in zircons of Group II eclogites are clinopyroxene (omphacite, augite, and diopside), garnet (in most cases almandine-rich), rutile, muscovite, phengite, quartz, kyanite, sillimanite, carbonate (dolomite, calcite), melilite, and hauyne (Fig. 7). Chemical compositions of garnet inclusions in zircons of Group II eclogites are also chemically distinct from the matrix garnet (Fig. 8 and Table 3).

4.2.1. Clinopyroxene

Chemical composition of clinopyroxene in matrix and as inclusion phase from both groups of eclogites is plotted on the WEF–Jd–Ae ternary diagram (Fig. 8a). Composition of clinopyroxene inclusions in zircons is more or less identical to the composition of clinopyroxene in matrix (Fig. 8a).

Chemical composition of clinopyroxene in matrix of Group II eclogites is slightly different from the clinopyroxene inclusions in zircons (Fig. 8a and Table 2). Clinopyroxene in matrix eclogite contains abundant quartz rods and exsolution lamellae (Fig. 3f). In addition, along the grain boundary they are retrogressed to amphibole and quartz–albite–jadeite symplectites (Fig. 3e). In contrast, clinopyroxene inclusions in zircon do not contain quartz rods or exsolution lamellae and they are aegirine-poor and jadeite-rich when compared with the matrix clinopyroxene (Table 2).

4.2.2. Garnet

Garnet inclusions in zircon are clear, transparent and single-phased with no fractures or retrograde features. However, in matrix most of the garnets are full of inclusions, cracked and embayed at rim portions where secondary amphibole and chlorite have developed. Chemical composition of garnets from both inclusions and matrix from both groups of eclogites is plotted on the Alm + Sps–Grs–Prp ternary diagram (Fig. 8b) and shown in Table 3. In Group I eclogites matrix garnets are homogenous and show slight zoning with decreasing grossularite component from core to rim. They are mainly almandine-rich. Chemical composition of garnet inclusions in zircons from Group I eclogites is also almandine-rich, however slightly different from the matrix garnet. Grossularite component is significantly higher in garnet inclusions in zircon compared with the matrix garnet (Table 3). Similar increase in the spessartine component is also observed.

Chemical composition of garnet inclusions in zircon from Group II eclogites is significantly different from the matrix garnet. They are mainly almandine-rich compared with matrix garnet (Fig. 8b).

5. Zircon U–Th–Pb Geochronology

To unravel the complex metamorphic history of the HP and UHP eclogites of the Kaghan Valley and to understand the protolith rocks of these eclogites zircons from these rocks were dated. Zircons from both groups of eclogites were analyzed for the U–Th–Pb age-dating with ion probe HR-SIMS Cameca-ims 1270. Analyzed spots on zircons are shown in Figs. 6 and 9 for Group II and I eclogites respectively (the number of analyzed zircons is large therefore representative grains are shown only). Geochronological results of each spot on zircons from both groups of eclogites are shown in Table 4 and the graphic illustration, on a Wetherill

Table 2
Chemical composition of clinopyroxene in eclogite matrix and as inclusions in zircons. Bdl means below detection limit.

Sample	Group I zrns							Matrix				Group II zrns							Matrix			
	Ph380A		Ph380B				Ph380D	Ph380D				Mount A		Mount B					Ph423			
Location	Omp46	Omp19	Omp12	Omp16	Omp27	Omp28	Omp11	Omp115	Omp116	Omp117	Omp118	Zrn1_18	Zrn1_19	Zrn12_69	Zrn16_84	Zrn19_85	Zrn31_93	Zrn4_65	cpx2_105	cpx2_106	cpx2_122	cpx2_124
SiO_2	54.16	54.12	54.62	55.05	54.55	54.69	54.32	55.79	55.46	56.00	55.38	55.46	55.75	54.92	55.02	55.36	55.03	56.15	54.66	56.50	56.15	56.48
Al_2O_3	7.51	7.44	7.69	7.53	7.81	7.54	7.67	8.51	8.04	8.07	8.06	9.60	9.53	9.58	9.64	9.70	9.89	9.34	9.79	9.75	9.59	9.67
Cr_2O_3	Bdl	Bdl	0.240	0.110	0.100	0.130	0.080	Bdl	0.021	0.044	0.004	0.070	0.240	0.180	0.100	0.240	0.080	0.080	0.030	0.010	0.050	0.050
TiO_2	0.23	0.24	0.25	0.13	0.08	0.11	0.12	0.07	0.14	0.14	0.22	0.30	0.05	0.02	0.22	0.23	0.11	Bdl	0.09	0.05	0.07	0.06
MgO	8.50	8.22	8.25	7.88	8.04	7.66	8.20	8.02	8.04	7.77	8.01	7.47	7.46	7.31	7.34	7.53	7.35	7.33	7.51	7.58	7.88	7.68
FeO	8.89	9.26	8.70	9.28	9.60	10.06	8.87	8.37	9.14	9.41	9.74	7.52	7.73	8.65	8.20	7.68	7.84	8.13	8.07	7.86	7.29	6.98
MnO	0.20	Bdl	0.01	Bdl	0.03	Bdl	Bdl	0.05	0.03	0.04	0.04	0.09	0.10	0.01	0.05	Bdl	0.20	Bdl	0.03	0.03	0.03	0.04
NiO	Bdl	Bdl	Bdl	Bdl	Bdl	Bdl	Bdl	0.13	0.04	0.06	Bdl	Bdl	Bdl	Bdl	Bdl	Bdl	Bdl	Bdl	0.26	0.06	0.03	Bdl
CaO	13.79	13.68	14.73	14.19	13.98	13.94	13.80	14.09	14.52	12.90	14.16	13.12	13.07	12.64	13.05	12.90	13.21	12.48	13.30	13.02	13.16	13.31
Na_2O	6.78	7.12	5.54	5.87	5.92	6.04	7.04	6.08	6.32	6.46	6.07	6.43	6.17	6.75	6.37	6.54	6.32	6.74	7.20	7.05	7.11	7.16
K_2O	Bdl	Bdl	Bdl	Bdl	Bdl	Bdl	Bdl	Bdl	Bdl	0.01	0.02	Bdl	Bdl	Bdl	0.01	Bdl	Bdl	Bdl	Bdl	Bdl	Bdl	Bdl
Total	100.06	100.08	100.03	100.04	100.11	100.17	100.10	101.11	101.75	100.90	101.71	100.06	100.10	100.06	100.00	100.18	100.03	100.25	100.94	101.91	101.36	101.43
TSi	1.945	1.941	1.983	1.998	1.977	1.984	1.947	1.995	1.971	2.008	1.975	1.998	2.014	1.978	1.986	1.993	1.985	2.020	1.941	1.990	1.982	1.992
TAl	0.055	0.059	0.017	0.002	0.023	0.016	0.053	0.005	0.029	–	0.025	–	–	0.022	0.014	0.007	0.015	–	0.059	0.010	0.018	0.008
M1Al	0.263	0.255	0.312	0.320	0.310	0.307	0.271	0.353	0.308	0.341	0.314	0.406	0.405	0.385	0.396	0.404	0.405	0.396	0.350	0.394	0.381	0.394
M1Ti	0.006	0.006	0.007	0.004	0.002	0.003	0.003	0.002	0.004	0.004	0.006	0.008	0.001	0.001	0.006	0.006	0.003	–	0.002	0.001	0.002	–
M1Fe_3	0.251	–	0.073	0.084	0.121	0.123	0.261	0.068	0.147	0.082	0.119	0.023	–	0.098	0.048	0.036	0.042	0.032	0.198	0.094	0.118	0.098
M1Fe_2	0.016	0.278	0.154	0.163	0.130	0.149	0.005	0.145	0.113	0.155	0.135	0.160	0.184	0.119	0.152	0.143	0.152	0.179	0.041	0.111	0.083	0.101
M1Cr	–	–	0.007	0.003	0.003	0.004	0.002	–	0.001	0.001	–	0.002	0.007	0.005	0.003	0.007	0.002	0.002	0.001	–	0.001	–
M1Mg	0.455	0.440	0.447	0.426	0.434	0.414	0.438	0.427	0.426	0.415	0.426	0.401	0.402	0.393	0.395	0.404	0.395	0.393	0.397	0.398	0.415	0.404
M1Ni	–	–	–	–	–	–	–	0.004	0.001	0.002	–	–	–	–	–	–	–	–	0.007	0.002	0.001	–
M2Fe_2	–	–	0.037	0.035	0.040	0.033	–	0.037	0.011	0.045	0.037	0.044	0.049	0.044	0.047	0.053	0.042	0.034	–	0.027	0.015	0.006
M2Mn	0.006	–	–	–	0.001	–	–	0.002	0.001	0.001	0.001	0.003	0.003	–	0.002	–0.003	0.006	–0.004	0.001	0.001	0.001	–
M2Ca	0.531	0.526	0.573	0.552	0.543	0.542	0.530	0.540	0.553	0.496	0.541	0.507	0.506	0.488	0.505	0.498	0.510	0.481	0.506	0.491	0.498	0.503
M2Na	0.472	0.495	0.390	0.413	0.416	0.425	0.489	0.421	0.435	0.449	0.420	0.449	0.432	0.471	0.446	0.457	0.442	0.470	0.496	0.481	0.487	0.490
Ca	52.643	42.294	47.320	46.909	47.280	47.601	54.487	46.907	50.085	44.566	47.455	45.475	44.211	46.746	45.856	45.489	46.156	44.393	53.508	47.800	49.232	49.529
Mg	45.148	35.360	36.876	36.245	37.834	36.394	45.048	37.123	38.576	37.349	37.349	36.025	35.111	37.615	35.886	36.945	35.733	36.279	42.039	38.720	41.017	39.764
Fe_2_Mn	2.209	22.346	15.803	16.846	14.886	16.004	0.466	15.970	11.339	18.085	15.196	18.500	20.677	15.639	18.257	17.566	18.111	19.328	4.453	13.479	9.751	10.708
JD1	17.828	14.692	19.498	20.140	19.835	19.616	18.536	22.494	20.014	21.839	20.132	26.044	25.845	25.455	25.622	26.066	26.269	25.446	24.291	26.115	25.438	26.170
AE1	14.203	13.796	4.869	5.851	6.777	7.565	14.932	4.339	8.288	6.979	6.860	2.643	1.412	5.523	3.257	3.171	2.376	4.640	10.124	5.803	7.076	6.388
CFTS1	2.813	–	0.129	–	1.145	0.545	3.100	–	1.322	–	0.754	–	–	1.278	0.041	–	0.515	–	3.711	0.438	0.869	0.244
CTTS1	0.422	0.373	0.427	0.110	0.140	0.192	0.221	0.125	0.242	–	0.380	0.103	–	0.036	0.387	0.402	0.194	–	0.167	0.088	0.124	0.106
WO1	32.764	29.873	35.244	34.607	33.442	33.926	32.929	34.245	34.375	31.757	33.551	32.407	32.247	30.961	32.231	31.689	32.409	31.055	31.250	32.046	32.261	33.093
EN1	30.873	25.287	27.898	26.825	27.788	26.502	29.971	27.201	27.680	26.614	27.299	25.754	25.610	25.970	25.558	26.064	25.639	25.279	27.598	26.384	27.705	26.849
FS1	1.098	15.980	11.936	12.468	10.874	11.654	0.310	11.597	8.079	12.811	11.024	13.049	14.887	10.778	12.904	12.609	12.599	13.702	2.861	9.126	6.526	7.151
Q	1.002	1.243	1.211	1.176	1.147	1.139	0.973	1.150	1.103	1.111	1.139	1.111	1.141	1.043	1.099	1.097	1.100	1.087	0.945	1.027	1.010	1.014
J	0.944	0.990	0.780	0.826	0.832	0.850	0.979	0.843	0.871	0.899	0.840	0.899	0.865	0.943	0.892	0.913	0.884	0.941	0.991	0.963	0.973	0.979
WO	42.153	42.294	44.626	43.799	42.774	42.958	42.947	44.287	44.190	41.497	42.982	44.543	44.211	42.745	43.935	44.050	44.457	43.139	44.227	43.801	44.105	45.156
EN	36.152	35.360	34.777	33.842	34.227	32.844	35.507	35.049	34.036	34.776	33.829	35.287	35.111	34.396	34.383	35.777	34.417	35.254	34.748	35.480	36.746	36.253
FS	21.695	22.346	20.597	22.358	22.999	24.198	21.546	20.664	21.774	23.727	23.190	20.170	20.677	22.859	21.681	20.173	21.127	21.607	21.025	20.719	19.150	18.591
WEF	51.631	55.656	60.821	58.742	57.982	57.257	49.848	57.733	55.901	55.299	57.577	55.350	56.966	52.534	55.244	54.504	55.578	53.539	48.817	51.631	50.949	50.907
JD	24.748	44.344	31.743	32.721	30.225	30.503	25.529	35.436	29.832	36.010	30.790	42.225	43.034	37.856	39.907	41.801	40.222	43.034	32.660	39.062	37.481	39.279
AE	23.621	–	7.436	8.537	11.793	12.240	24.622	6.831	14.267	8.691	11.634	2.425	–	9.610	4.849	3.695	4.200	3.427	18.522	9.307	11.570	9.814

Compositions were calculated on the basis of 4 cat ions and 6 oxygen atoms.

Table 3
Chemical composition of garnet in eclogite matrix and as inclusions in zircons. Bdl means below detection limit.

Sample	Grt incl in Group I Zrns			Matrix Grt in Group I				Grt incl in Group II Zrns								Matrix Grt in Group II			
	Ph380D	Ph380D	Ph380D				MountA				MountB				Ph423				
Location	grt1	grt32	grt1–3	grt1–7	grt1–8	grt1–12	Zrn19–23	Zrn19–24	Zrn19–25	Zrn19–29	Zrn2–76	Zrn23–63	Zrn4–77	Zrn15–89	grt1_14	grt1_17	grt1_24	grt2_54	grt2_64
SiO_2	38.82	39.10	38.38	39.72	39.18	39.05	38.04	38.09	38.25	39.79	39.38	38.37	39.10	40.61	39.80	39.71	38.36	40.65	39.11
TiO_2	0.04	0.03	0.03	0.06	0.01	0.01	0.02	0.08	0.17	0.00	Bdl	0.14	Bdl	Bdl	Bdl	0.03	0.05	0.12	0.03
Al_2O_3	20.04	21.06	21.02	21.77	21.95	22.07	20.52	20.21	19.98	19.61	20.26	20.84	20.70	19.66	22.95	22.46	21.58	22.54	21.58
Cr_2O_3	Bdl	Bdl	0.024	0.004	0.020	0.022	0.040	0.210	0.060	0.080	0.010	Bdl	Bdl	0.090	0.010	0.040	0.010	0.060	0.070
FeO	26.29	26.71	28.28	27.39	28.18	28.48	28.03	27.88	26.87	27.03	25.83	26.66	26.13	25.74	21.65	22.00	21.47	19.71	21.21
MnO	0.91	1.09	0.54	0.43	0.41	0.42	1.00	0.90	0.77	0.92	0.55	0.79	0.67	0.65	0.48	0.46	0.47	0.45	0.40
MgO	3.37	4.22	5.46	5.20	5.35	5.23	3.90	3.85	4.33	3.92	4.92	4.30	5.30	4.24	8.59	7.87	8.41	8.47	8.11
CaO	7.66	7.72	7.25	6.32	7.06	6.43	8.40	8.81	9.63	8.71	9.18	9.12	8.15	9.12	9.38	9.01	9.56	9.57	9.38
Na_2O	0.03	0.13	0.08	0.07	0.05	0.02	0.07	0.01	0.02	0.00	0.03	0.04	0.07	0.05	0.04	0.00	0.00	0.02	0.02
Total	97.16	100.06	101.06	100.96	102.19	101.74	100.02	100.04	100.08	100.06	100.16	100.26	100.12	100.16	102.90	101.58	99.91	101.59	99.91
FeO calc.	26.290	26.710	26.867	26.021	26.768	27.052	26.540	26.689	25.232	27.030	25.830	26.131	25.940	25.740	19.687	21.567	18.290	19.710	19.912
Fe_2O_3 calc.	–	–	1.571	1.522	1.565	1.582	1.656	1.324	1.821	–	–	0.588	0.211	–	2.182	0.481	3.534	–	1.442
TSi	3.153	3.067	2.971	3.075	2.997	3.005	2.999	3.006	3.006	3.136	3.074	3.009	3.049	3.186	2.941	2.986	2.924	3.036	2.984
TAl	–	–	0.029	–	0.003	–	0.001	–	–	–	–	–	–	–	0.059	0.014	0.076	–	0.016
Sum_T	3.153	3.067	3.000	3.075	3.000	3.005	3.000	3.006	3.006	3.136	3.074	3.009	3.049	3.186	3.000	3.000	3.000	3.036	3.000
AlVI	1.917	1.945	1.888	1.985	1.974	2.000	1.903	1.879	1.849	1.820	1.863	1.924	1.901	1.817	1.937	1.975	1.861	1.982	1.923
Fe_3	–	–	0.091	0.089	0.090	0.091	0.098	0.079	0.108	–	–	0.035	0.012	–	0.121	0.027	0.203	–	0.083
Ti	0.002	0.002	0.002	0.004	–	0.001	0.001	0.005	0.010	–	–	0.008	–	–	–	0.002	0.003	0.007	0.002
Cr	–	–	0.001	–	0.001	0.001	0.002	0.013	0.004	0.005	0.001	–	–	0.006	0.001	0.002	0.001	0.004	0.004
Sum_A	1.919	1.947	1.983	2.077	2.066	2.094	2.005	1.975	1.970	1.825	1.858	1.962	1.907	1.811	2.059	2.006	2.067	1.993	2.012
Fe_2	1.786	1.752	1.740	1.685	1.712	1.741	1.750	1.762	1.658	1.782	1.686	1.714	1.692	1.689	1.216	1.356	1.166	1.231	1.270
Mg	0.408	0.493	0.630	0.601	0.610	0.600	0.458	0.453	0.507	0.461	0.573	0.503	0.616	0.496	0.946	0.882	0.956	0.943	0.922
Mn	0.063	0.072	0.036	0.028	0.026	0.028	0.067	0.060	0.051	0.061	0.036	0.052	0.044	0.043	0.030	0.029	0.030	0.028	0.026
Ca	0.667	0.649	0.601	0.524	0.578	0.530	0.709	0.745	0.811	0.735	0.768	0.766	0.681	0.767	0.743	0.726	0.781	0.766	0.767
Na	0.005	0.020	0.011	0.010	0.007	0.003	0.011	–	–	–	0.005	–	0.011	0.008	0.006	–	–	0.003	0.003
Sum_B	2.928	2.986	3.017	2.848	2.934	2.902	2.995	3.018	3.024	3.039	3.068	3.029	3.044	3.003	2.941	2.994	2.933	2.971	2.988
Alm	60.487	58.416	47.963	59.370	58.497	60.058	58.630	57.467	53.479	54.113	50.788	55.082	53.312	52.273	41.443	36.196	35.316	41.473	34.027
And	–	–	5.641	4.686	4.617	4.740	4.938	3.986	5.487	–	–	1.770	0.648	–	6.200	1.591	11.133	–	4.778
Gross	23.160	22.211	18.975	13.767	15.076	13.488	18.711	20.534	21.870	26.566	27.413	24.277	23.054	27.716	19.068	26.556	17.419	25.619	24.474
Pyrope	14.177	16.893	25.868	21.166	20.849	20.694	15.358	15.314	17.234	16.807	20.467	17.088	21.446	18.127	32.235	34.377	34.988	31.770	35.483
Spess	2.175	2.479	1.463	0.998	0.899	0.951	2.237	2.034	1.741	2.241	1.300	1.784	1.540	1.579	1.023	1.142	1.111	0.959	0.994
Uvaro	–	–	0.091	0.013	0.062	0.069	0.125	0.664	0.190	0.273	0.033	–	–	0.306	0.030	0.139	0.033	0.179	0.244
XCagnt	0.228	0.219	0.200	0.185	0.198	0.183	0.238	0.247	0.268	0.242	0.251	0.252	0.225	0.256	0.253	0.243	0.266	0.258	0.257
XFegnt	0.611	0.591	0.579	0.594	0.585	0.601	0.586	0.583	0.548	0.586	0.550	0.565	0.558	0.564	0.414	0.453	0.398	0.415	0.425
XMggnt	0.140	0.166	0.210	0.212	0.208	0.207	0.153	0.150	0.167	0.152	0.187	0.166	0.203	0.166	0.322	0.295	0.326	0.318	0.309
Fe_Mggnt	4.377	3.554	2.762	2.804	2.807	2.902	3.821	3.890	3.270	3.866	2.942	3.408	2.747	3.405	1.285	1.537	1.220	1.305	1.377

Grt calculated on the basis of 8 cat ions and 12 oxygen atoms.

Table 4
HR-SIMS Cameca-ims 1270 in situ zircon U–Th–Pb data of the Himalayan HP and UHP eclogites. The term "disc" in the table means discordant.

Sample	Zircon	Contents (ppm)		Th/U	$^{207}Pb/^{206}Pb$	Error	$^{207}Pb/^{235}U$	Error	$^{206}Pb/^{238}U$	Error	Rho	$^{206}Pb/^{204}Pb$	(Age (Ma ± 2σ)
	Domain	U	Th			2σ		2σ		2σ			$^{207}Pb/^{235}U$)
Group I													
Ph380A													
Zr3@1	Core	115	63	0.546	0.0554	0.0003	0.2549	0.0364	0.0209	0.0007	0.479	646.12	Disc
Zr3@2	Center	97	104	1.071	0.0644	0.0042	0.3872	0.0277	0.0423	0.0003	−0.359	1388.94	Disc
Zr3@3	Rim	70	64	0.916	0.0771	0.0059	0.4178	0.0354	0.0382	0.0004	−0.326	672.52	Disc
Zr5@1	Core	25	15	0.576	0.0769	0.0097	0.3484	0.0568	0.0289	0.0005	0.237	365.13	Disc
Ph380B													
Zr1@1	Core	313	437	1.399	0.0539	0.0007	0.2977	0.0495	0.0401	0.0039	0.871	4551.54	248 ± 22
Zr1@2	Core	259	365	1.409	0.0535	0.0005	0.3254	0.0351	0.0438	0.0022	0.866	7449.63	272 ± 11
Zr1@3	Rim	94	75	0.799	0.0519	0.0014	0.2158	0.0518	0.0302	0.0018	0.459	746.68	191 ± 11
Zr1@5	Core	1579	2711	1.717	0.0521	0.0003	0.2957	0.0225	0.0411	0.0023	0.980	16804.65	253 ± 10
Zr1@6	Center	977	1339	1.371	0.0518	0.0005	0.2500	0.0232	0.0345	0.0018	0.961	8865.33	210 ± 07
Zr3@1	Rim	96	128	1.326	0.0540	0.0014	0.3143	0.0097	0.0422	0.0005	0.836	1251.06	Disc
PH380D													
Zr1@1	Core	25	28	1.092	0.0542	0.0014	0.2968	0.0661	0.0390	0.0021	0.709	1946.55	244 ± 11
Zr1@2	Core	12	12	0.999	0.0523	0.0015	0.2891	0.0661	0.0401	0.0024	0.670	786.35	252 ± 13
Zr1@3	Core	27	22	0.820	0.0518	0.0011	0.3050	0.0601	0.0420	0.0019	0.789	2953.08	264 ± 09
Zr1@4	Core	48	63	1.323	0.0543	0.0011	0.3390	0.0689	0.0443	0.0025	0.717	657.73	276 ± 01
Zr1@5	Rim	32	28	0.860	0.0606	0.0024	0.1568	0.0564	0.0186	0.0016	0.434	143.23	117 ± 09
Zr7@1	Core	17	11	0.633	0.0532	0.0015	0.2698	0.0671	0.0370	0.0017	0.557	1540.05	233 ± 09
Zr8@1	Rim	40	35	0.876	0.0727	0.0037	0.3162	0.2926	0.0279	0.0039	0.694	879.52	170 ± 19
Zr8@2	Center	43	46	1.076	0.0565	0.0015	0.2310	0.0497	0.0297	0.0016	0.418	1550.19	187 ± 10
Zr8@3	Rim	63	51	0.821	0.0566	0.0015	0.1857	0.0729	0.0227	0.0021	0.911	2335.78	139 ± 06
Zr12@2	Rim	10	6	0.634	0.0863	0.0087	0.3076	0.3696	0.0215	0.0040	0.841	298.76	127 ± 15
Zr13@1	Center	11	5	0.433	0.0540	0.0022	0.1977	0.0655	0.0263	0.0021	0.605	575.88	166 ± 12
Zr13@2	Rim	32	8	0.261	0.0527	0.0020	0.0808	0.0237	0.0111	0.0009	0.178	703.27	71 ± 06
Zr14@1	Core	31	32	1.041	0.0538	0.0014	0.2755	0.0625	0.0381	0.0020	0.567	1784.42	241 ± 11
Zr16@1	Center	12	9	0.729	0.0550	0.0023	0.2068	0.0799	0.0275	0.0025	0.445	536.95	174 ± 15
Zr17@1	Rim	53	41	0.775	0.0599	0.0023	0.1477	0.1451	0.0163	0.0018	0.447	1048.97	103 ± 11
Zr19@1	Core	301	403	1.340	0.0600	0.0018	0.3701	0.1146	0.0428	0.0007	0.933	4791.97	267 ± 02
Group II Mount A													
A_Ph423_07@01	Center	5.96	0.07	0.011	0.0707	0.0074	0.0736	0.0629	0.0071	0.0014	0.196	51.00	45.5 ± 8.8
A_Ph423_07@02	Rim	5.49	0.06	0.011	0.0530	0.0064	0.0559	0.0559	0.0070	0.0017	0.175	51.45	45.0 ± 11
A_Ph423_10@03	Center	9.92	0.44	0.044	0.0521	0.0053	0.0461	0.0375	0.0062	0.0014	0.123	87.71	39.7 ± 8.7
A_Ph423_15@04	Center	5.39	0.16	0.030	0.0597	0.0056	0.0610	0.0489	0.0069	0.0012	0.026	45.10	44.5 ± 7.7
A_Ph425_02@05	Center	1.37	0.00	0.003	0.1148	0.0205	0.1334	0.1848	0.0075	0.0040	0.143	12.46	Disc
A_Ph425_03@07	Center	2.58	0.04	0.014	0.0923	0.0136	0.0996	0.1083	0.0072	0.0026	0.281	24.13	45.0 ± 16
A_Ph425_03@08	Center	2.57	0.02	0.009	0.0771	0.0130	0.0915	0.1242	0.0074	0.0024	0.320	19.07	46.0 ± 15
A_Ph425_03@09	Rim	3.15	0.02	0.007	0.0737	0.0109	0.0859	0.0930	0.0074	0.0025	0.327	26.82	46.0 ± 16
A_Ph425_05@10		1.82	0.01	0.006	0.0689	0.0127	0.0782	0.1290	0.0070	0.0031	0.295	17.60	44.0 ± 19
A_Ph425_06@11		1.34	0.01	0.006	0.0807	0.0165	0.0918	0.1356	0.0070	0.0033	0.250	10.70	44.0 ± 21
A_Ph425_06@12		0.94	0.01	0.016	0.0923	0.0236	0.1104	0.1969	0.0075	0.0042	0.081	9.39	Disc
A_Ph425_11@14	Rim	144	1.78	0.012	0.0493	0.0012	0.0485	0.0121	0.0071	0.0019	0.812	1023.46	47.0 ± 11
A_Ph425_11@15	Center	268	3.59	0.013	0.0496	0.0009	0.0505	0.0087	0.0073	0.0005	0.798	3027.11	45.9 ± 2.4
A_Ph425_19@17	Center	166	6.26	0.038	0.0567	0.0014	0.0584	0.0119	0.0074	0.0006	0.670	1488.24	45.8 ± 3.6
A_Ph425_20@18	Center	10.18	0.06	0.005	0.0575	0.0050	0.0633	0.0493	0.0072	0.0011	0.550	92.17	45.0 ± 6.5
A_Ph425_24@19	Center	144	1.28	0.009	0.0490	0.0012	0.0476	0.0094	0.0071	0.0009	0.817	1425.93	45.3 ± 5.1
A_Ph425_24@20	Rim	55	0.43	0.008	0.0514	0.0020	0.0467	0.0161	0.0066	0.0008	0.597	439.84	41.7 ± 4.7
A_Ph425_26@21	Center	82	1.33	0.016	0.0479	0.0016	0.0483	0.0140	0.0073	0.0008	0.623	698.04	46.6 ± 4.9
Group II Mount B													
B_Ph425_19@01	Center	3.18	0.03	0.008	0.1073	0.0160	0.1038	0.1179	0.0074	0.0029	0.296	13.07	46.0 ± 18
B_Ph425_17@02	Center	1.17	0.05	0.040	0.0704	0.0148	0.0810	0.1245	0.0072	0.0027	−0.085	10.52	Disc

B_Ph425_16@03	Center	1.83	0.02	0.011	0.0728	0.0130	0.0835	0.1220	0.0070	0.0022	0.238	19.56	44.0 ± 14
B_Ph425_14@04	Center	1.43	0.01	0.005	0.1332	0.0214	0.1453	0.1932	0.0068	0.0027	0.082	12.15	44.0 ± 17
B_Ph425_02@06	Center	83	2	0.018	0.0538	0.0017	0.0500	0.0138	0.0067	0.0006	0.515	549.27	42.8 ± 3.6
B_Ph425_04@07	Center	228	7	0.033	0.0498	0.0019	0.0564	0.0407	0.0076	0.0026	0.898	1060.32	46.0 ± 11
B_Ph425_06@09	Center	4.40	0.05	0.011	0.0654	0.0091	0.0630	0.0730	0.0066	0.0019	0.068	31.62	43.0 ± 12
B_Ph425_07@10	Center	9.25	0.12	0.013	0.0555	0.0048	0.0552	0.0463	0.0067	0.0012	0.180	75.11	43.2 ± 7.5
B_Ph425_08@11	Center	1.81	0.02	0.011	0.0955	0.0209	0.1092	0.1692	0.0070	0.0029	0.222	13.55	44.0 ± 19
B_Ph425_11@13	Center	246	2	0.009	0.0494	0.0010	0.0457	0.0096	0.0068	0.0008	0.511	1727.66	44.0 ± 4.8
B_Ph425_18@14	Center	131	7	0.050	0.0595	0.0022	0.0566	0.0235	0.0069	0.0013	0.779	643.92	41.2 ± 6.7
B_Ph425_26@15	Center	259	11	0.042	0.0475	0.0009	0.0417	0.0078	0.0063	0.0006	0.915	1950.69	40.0 ± 2.6
B_Ph423_18@16	Center	20	0.34	0.017	0.0599	0.0038	0.0581	0.0330	0.0067	0.0009	0.010	155.23	43.4 ± 5.5
B_Ph422_01@19	Center	6.37	0.20	0.031	0.0593	0.0055	0.0548	0.0513	0.0065	0.0017	0.598	51.63	40.0 ± 10
B_Ph422_02@20	Center	1.65	0.04	0.024	0.1410	0.0224	0.1442	0.1720	0.0067	0.0030	0.022	14.74	44.0 ± 19
B_Ph422_05@21	Center	8.94	0.32	0.035	0.0688	0.0083	0.0685	0.0715	0.0067	0.0017	0.303	72.67	43.0 ± 11
B_Ph422_06@22	Center	20	0.25	0.013	0.0555	0.0040	0.0683	0.1607	0.0068	0.0014	0.679	227.30	42.7 ± 6.8
B_Ph422_07@23	Center	5.69	0.44	0.077	0.0737	0.0077	0.0713	0.0656	0.0062	0.0014	0.170	53.91	39.9 ± 8.7

Concordia diagram, is shown in Fig. 10. Several points with large age errors are removed from the diagram. Zircon age-dating was assisted by phase assemblage of micro-inclusions, zircon internal structures and zoning pattern. Mineral inclusions in each discrete zoned domain in zircon were identified in order to determine progressive, peak and retrogressive stages of metamorphism preserved in these zircons. This information along with zircon morphology and internal structures via CL imaging enabled us to differentiate magmatic zircons (protolith-related) from the metamorphic ones and metamorphic evolution of their precursors.

5.1. Group I eclogites

Twenty-eight analyses of the zircons from Group I (Samples Ph380A, Ph380B, and Ph380D) were carried out for the U–Th–Pb isotope ratios (Table 4). For large zircon grains, 3–4 spots were analyzed at middle and rim portions, whereas smaller grains were analyzed for a single spot. The U–Th–Pb isotopic data for most of the core portions of zircon in Group I eclogites are concordant. However the middle and rim portions in several zircons yielded discordant age values which were significantly older than the age of the Himalayan eclogite-facies event. The radiometric dates, obtained from the core portions bracket between 244 and 276 Ma with a concordant age of 267.1 ± 2.4 Ma (MSWD = 8.5) (Fig. 10b). Several other spots show a wide scatter in age bracketing between 210 and 71 Ma (Table 4).

5.2. Group II eclogites

From Group II eclogites 114 zircon grains were separated. Most of these grains were very small and they had low U, Th and Pb contents therefore were not possible for age-dating using the HR-SIMS. However among them 34 grains, which contained suitable amount of U, Th and Pb, were analyzed for 42 spots. These zircons were picked from three eclogitic samples, namely Ph422, Ph423 and Ph425, of UHP grade. Zircons were mounted on two rounded discs (2.5 cm in diameter) made of epoxy resin. These discs were referred to as mount A and B respectively. A few larger grains were analyzed for two to three spots on a CL-dark and CL-bright portions, whereas several other smaller grains were analyzed for a single spot. The age data obtained from the CL-dark and CL-bright portions did not vary significantly. The U–Th–Pb age, obtained from zircons of Group II eclogites lie in a narrow range between 47 and 40 Ma, with a concordant result of 44.9 ± 1.2 Ma (MSWD = 4.9) (Fig. 10c). Their weighted average mean was 44.5 Ma (see inlet in Fig. 10c). Because those zircons contained micro-inclusions such as garnet, omphacite and phengite, they have clearly been recrystallized under the peak eclogite-facies stage from the precursor fluids enriched with Zr and Si contents. Several grains yielded apparently younger age ca. 39.7 ± 8.7 Ma, which probably reveal late-stage recrystallization or growth from the older zircons. All the zircon grains in Group II eclogites have lower U and Th contents and the Th/U ratios are less than 0.05 (Table 4), indicating that they are typically metamorphic in origin (Hoskin and Black, 2000).

6. Interpretation of results

6.1. Igneous versus metamorphic zircons

Zircons occur in eclogites mainly as either inherited from the oceanic protolith or formed due to metamorphism (Rubatto, 2002). Hence, the origin of zircon extracted from eclogites needs to be investigated prior to geologic interpretation of the age. The presence of mineral inclusions and their chemical compositions

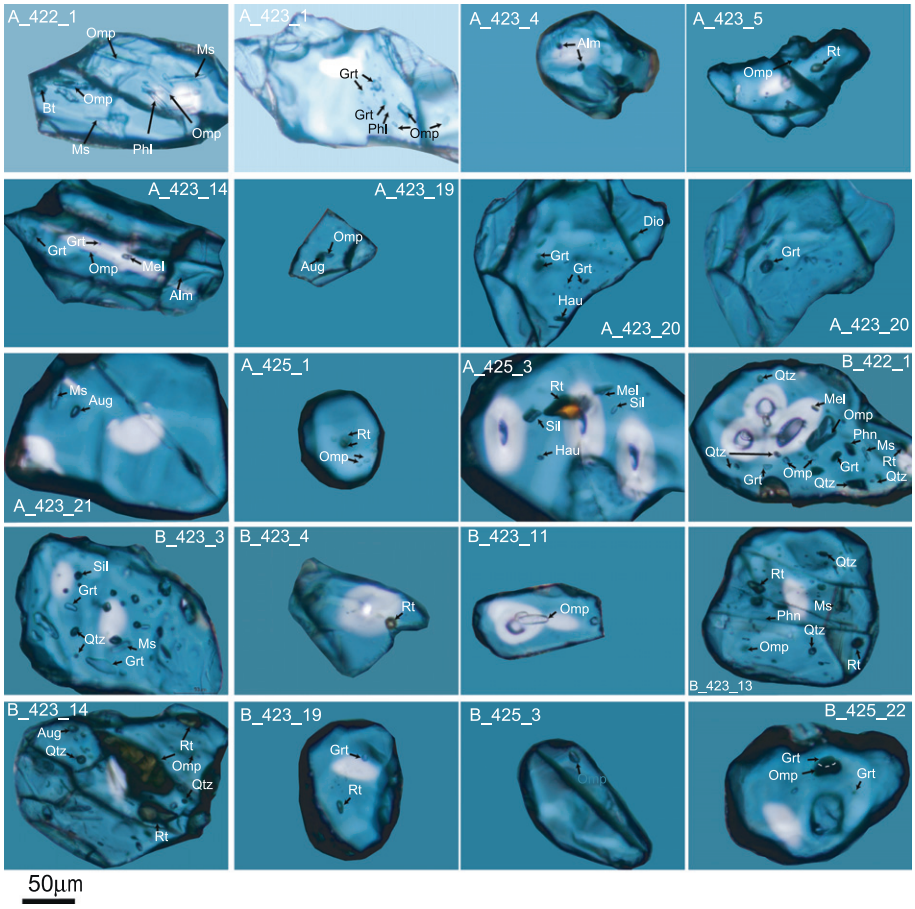

Fig. 7. Micro-inclusions assemblage in zircons of Group II eclogites. All the inclusions were identified using micro-Raman spectroscopy. Inclusions exposed at the zircon surface were also identified and analyzed using SEM-EDX detector.

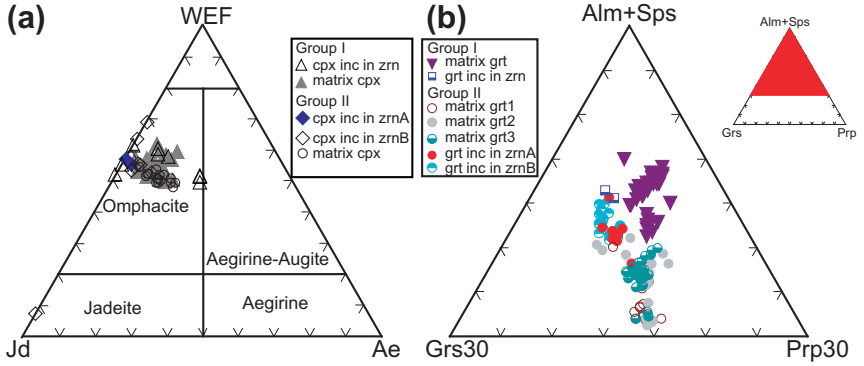

Fig. 8. Chemical composition of clinopyroxene (a) and garnet (b) inclusions in zircon and matrix plotted on WEF–Jd–Ae and Alm + Sps–Grs–Prp ternary diagrams respectively. Abbreviations WEF: wollastonite–enstatite–ferrosilite; Jd: jadeite; Ae: aegirine; Alm: almandine; Sps: spessartine; Grs: grossularite; Prp: pyrope.

play important role to distinguish between inherited magmatic zircons from metamorphic ones. Combined with the CL image information, textural features and mineral inclusions, the U–Th–Pb geochronology help to refine the origin of zircons found in the Himalayan eclogites. The higher Th/U ratios of zircons in Group I eclogites in the middle portions with a U–Th–Pb age of 267 Ma indicate their inheritance within igneous protolith. Whereas the lower Th/U ratio (<0.05, Table 4) of the metamorphic zircons from Group II eclogites (with a U–Th–Pb age of 45 Ma) suggest that these zircons grew during metamorphism. This is because U is more mobile than Th, and during metamorphism the external fluids provide more U, thus Th/U ratio lowers in metamorphic zircons (Rubatto et al., 1999; Zheng et al., 2006).

6.2. Occurrence of zircon and its formation environments

The presence of inherited zircon in mafic rocks (basalts) can be explained either by recycling of continental material into the mantle source, or formation of zircon in the metasomatised mantle (Rubatto, 2002). Zircon occurs commonly either as a precipitate

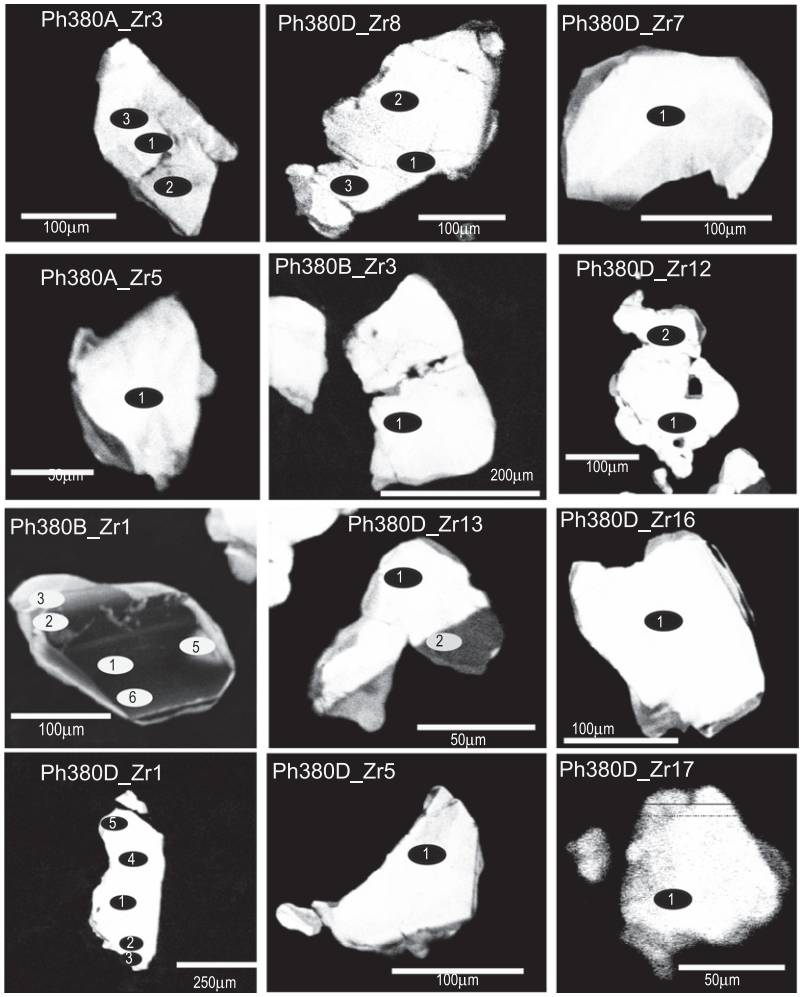

Fig. 9. Cathodoluminescence (CL) images of in situ zircons of Group I eclogites. Numbered ellipses represent position of the HR-SIMS Cameca-ims 1270 spot measured for the U–Th–Pb age-dating.

from a melt or as a result of metamorphism. The igneous zircons in Group I eclogites may have precipitated from melt or inherited from the crustal component during mixing with magma. Contrary to that, the metamorphic zircons in Group II could have precipitated from metamorphic fluids, formed by the breakdown of other minerals and utilizing their Zr and Si contents, or recrystallized from the original igneous protolith zircons (Hoskin and Black, 2000; Whitehouse and Kamber, 2003). The radiometric age data of zircons, supported by CL imaging and micro-inclusion assemblages and their chemical composition, enabled us to distinguish between the protolith-related igneous zircons and the recrystallized phases of zircons which were grown during different stages of subduction-related metamorphism and subsequent exhumation. The U–Th–Pb zircon concordant age of 267.1 ± 2.4 Ma very likely corresponds to the zircon crystallization age, establishing a magmatic origin for the zircons. This age is assumed to be the age of initial magmatic activity in the Himalayan region, which consequently gave rise to the eclogite protolith. Our results from zircons within eclogites are consistent with previous age results (e.g., a Rb–Sr pseudo-isochron of 264 Ma by Honegger et al. (1982); a U–Pb zircon age of 269 Ma by Spencer and Gebauer (1996); and a U–Pb zircon SHIRIMP age of 253 Ma from felsic gneisses by Kaneko et al. (2003)). We interpret the 267 Ma as the timing of the initiation of magmatic activity at the Tethyan shelf margin during the Permian. The discordant results from the middle portions of zircon, ranging between 210 and 71 Ma, suggest that these zircons have been affected by one or more Pb-loss events before or during the HP and UHP eclogite-facies metamorphism. Moreover, the presence of larger grains of zircon in Group I eclogites and their typical igneous-type zoning pattern indicate a gabbroic protolith for these zircons. Our interpretation is supported by the Fe–Ti-rich whole-rock chemical composition of the Group I eclogites (see Rehman et al. (2008) for bulk rock chemical compositions). Consequently, our geochemical results suggest that the Himalayan eclogites are not only the products of basaltic flows but were also derived from intrusive dikes or sills of gabbroic composition.

The 44.9 ± 1.2 Ma concordant age from zircons of Group II eclogites reveal their growth during eclogite-facies metamorphism. We did not find any UHP minerals such as coesite or diamond in those zircons. However, coesite inclusion in matrix omphacite in the same rock sample (Ph423) clearly indicates that these zircons were formed at UHP-stable conditions during 45–46 Ma.

6.3. Pressure–temperature–time path

Fig. 11 illustrates the pressure–temperature–time path recorded in the Himalayan eclogites. The Kaghan valley eclogites were derived from the Panjal Trap continental basalts of Permian to Early Triassic age (Honegger et al., 1982). The basaltic activity took place at 267 Ma as seen from the geochronological results in this study. The intermediate age values (210–71 Ma) suggest

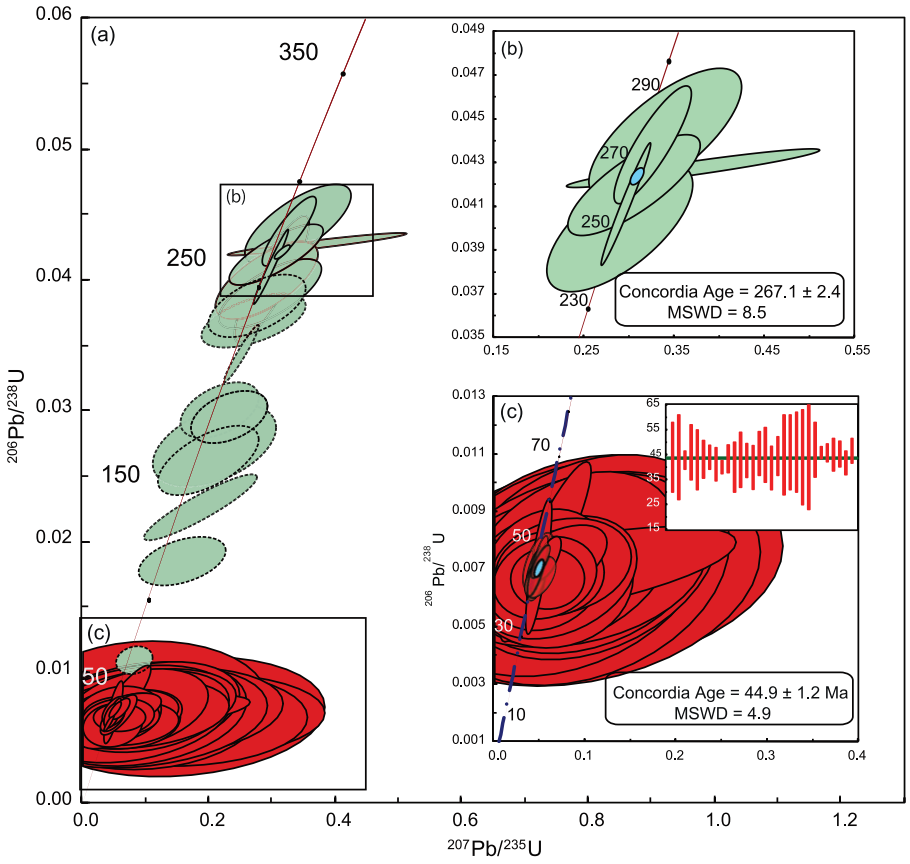

Fig. 10. (a) Ion probe U–Th–Pb zircon age data from zircons of Group I and II eclogites plotted on the Wetherill Concordia diagram. Age data of zircons from Group I eclogites after ca. 233 Ma (ellipses with dashed lines along the Concordia) indicate various amounts of Pb-loss events. (b) Wetherill Concordia diagram of zircons from Group I eclogites with a concordant value of 267.6 ± 2.4 Ma indicating the protolith emplacement age. (c) Wetherill Concordia diagram of zircons from Group II eclogites with a concordant age at 44.9 ± 1.2 Ma indicating the Himalayan eclogite-facies metamorphism. A histogram constructed at an average age value of 44.5 Ma is shown in an inlet in the upper right. All data-point errors are 2σ.

possible Pb-loss by the recrystallization or growth of new zircon domains from the older ones. This could have occurred during the Himalayan HP and UHP eclogite-facies metamorphism in the Paleogene. Closure of the Tethys Sea and transformation of the Panjal Trap basalts and gabbroic rocks into eclogites started with the initiation of the India-Asia collision at about 55–50 Ma (Patriat and Achache, 1984; Klootwijk et al., 1992; Beck et al., 1995). Eclogite-facies metamorphism in the leading-edge of the Indian Plate initiated at 49 ± 6 Ma (Tonarini et al., 1993) when these rocks reached to a depth of about 60–70 km. The jadeite, albite and quartz inclusions in several zircons represent this event. The process of eclogite-facies metamorphism continued and the rocks experienced UHP metamorphic event at 45 Ma (represented by filled star in Fig. 11) when the subducting slab of the Indian Plate gained a depth of >90 km. This event is confirmed by the U–Th–Pb zircon concordant age obtained from zircons of Group II eclogites (UHP) and from coesite-bearing zircons within felsic rocks which are located close to the UHP eclogite body. Since, no coesite was reported from Group I eclogites which lie to the south of Group II eclogites and slightly away from the subduction front, we presume that they experienced HP eclogite-facies metamorphism and did not cross the coesite stability field (subducted less than 90 km) (Fig. 11, filled rectangle marked with Group I). Our results are consistent with the previous age data reported from the felsic rocks and eclogites of the Kaghan Valley ca. 49 Ma Sm–Nd garnet-clinopyroxene isochron age from eclogites (Tonarini et al., 1993), 44 ± 3 Ma U–Pb zircon SHIRIMP age from eclogites (Spencer and Gebauer 1996), 46.2 ± 0.7 Ma U–Pb zircon SHIRIMP age from coesite-bearing zircons in felsic gneisses located close to the Group II eclogites (Kaneko et al., 2003), 46.4 ± 0.1 Ma U–Pb zircon and titanite from eclogites (Parrish et al., 2006) and 47.3 ± 0.4, 44.1 ± 1.3, and 41.3 ± 4.7 Ma U–Pb LA-ICMS age from zircon in felsic rocks and rutile and titanite in eclogites respectively (Wilke et al., 2010b). The short time span between initiation of eclogite-facies event ca. 49 Ma (Tonarini et al., 1993), to the UHP event ca. 46 Ma, until the amphibolite-facies event ca. 40 Ma (Wilke et al., 2010b) indicate rapid subduction after the eclogite-facies event, reached to UHP-stable stage, and exhumed back to amphibolite-facies stage rapidly. This could be because of the probable slab break-off (?) in the subducting Indian Plate leading-edge. The late-stage Barrovian metamorphism comprises an older (ca. 30 Ma) kyanite-bearing stage, followed by a younger (ca. 13–20 Ma) lower pressure, but higher temperature, sillimanite-bearing stage (O'Brien et al., 2001 and references therein) took place well after the major deformation occurred in the Himalayan region. This late-stage metamorphism overprinted most of the earlier thermal records in felsic rocks however retained partially in the mafic portions, i.e., eclogite bodies.

7. Conclusion

The well-developed, prismatic, and zoned zircon crystals in Group I eclogites with higher U and Th contents and high Th/U ratios (>1.72) indicate igneous origin. They preserve protolith-related features and hence represent the emplacement age of their

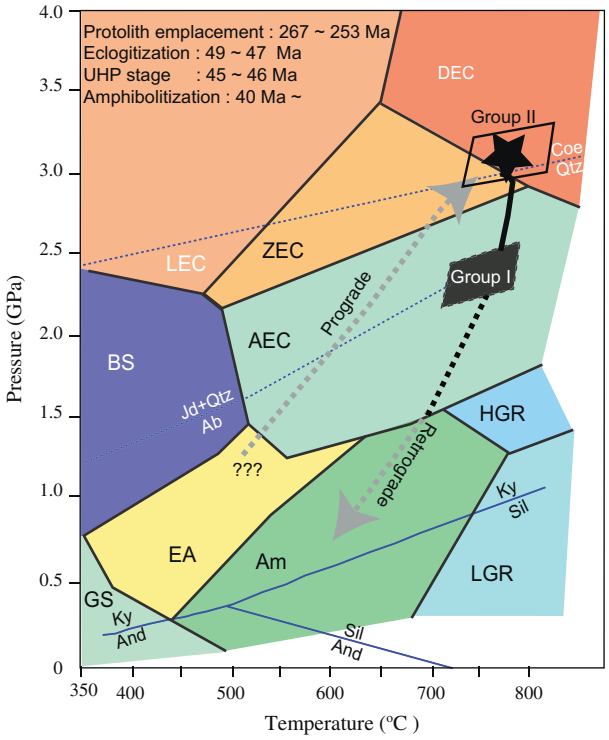

Fig. 11. Diagram illustrating the Pressure–Temperature–time path for the Himalayan HP (Group I) and UHP (Group II) eclogites. Prograde path is deduced from the inclusion assemblage in zircon of Group I eclogites as well as from the inclusions (quartz, albite and jadeite) in garnet. Filled star with rectangle represent the UHP peak event in Group II eclogites, deduced from mineral inclusions in zircon and geothermobarometry (coesite-present phase) from the matrix mineral assemblage. Filled rectangle represents HP stage in Group I eclogites, deduced from main mineral assemblage such as garnet, clinopyroxene, quartz, epidote and amphibole. Retrograde path with possible decompression stage is represented by a dashed-line. The path of metamorphism follows a clockwise pattern. Metamorphic facies boundaries and reaction curves are same as explained in Rehman et al. (2007). Abbreviations: AM, amphibolite-facies; BS, blueschist-facies; EA, epidote–amphibolite-facies; GS, greenschist-facies; HGR, high-pressure granulite-subfacies; LGR, low-pressure granulite-subfacies; AEC, amphibole-eclogite-subfacies; DEC, dry-eclogite-subfacies; LEC, lawsonite-eclogite-subfacies; ZEC, zoisite-eclogite-subfacies.

precursor rocks. The zircon U–Th–Pb concordant age at 267.1 ± 2.4 Ma thus correspond to the protolith formation in the Early Permian. The pre- and syn-metamorphic overgrowths in most zircon grains were obliterated by partial recrystallization and overgrowth. The zircon middle portions with intermediate and discordant age values between 210 and 71 Ma represent growth phases or possible Pb-loss during recrystalization of the older zircons during the continent–continent collision and the subsequent Himalayan eclogite-facies metamorphism. Micro-inclusion assemblage such as omphacite, garnet and phengite in the metamorphic zircons favor the notion that a fraction of these zircons were formed under the peak or UHP eclogite-facies stage yielding a concordant U–Th–Pb age of 44.9 ± 1.2 Ma, whereas several other domains (~40 Ma) were formed in the post-peak stage at higher temperature sufficient for zircon growth during early but retrograde stages of metamorphism.

Acknowledgments

First author is grateful to Dr. Tomohiro Usui for his help in sample preparation and laboratory techniques. Researchers and graduate students of the PML are also thanked for their valuable comments and discussion. Thanks to Ms. Tayyaba for reading the final draft. This work was carried out under the Visiting Researcher's Program of the Institute for the Study of the Earth's Interior, Okayama University. Part of this project was supported by the Ministry of Education, Culture, Sports, Science and Technology to H.Y. (KAKENHI 22540472).

References

Arnaud, N.O., Kelley, S.P., 1995. Evidence for excess Argon during high pressure metamorphism in the Dora Maira (Western Alps, Italy) using an ultra-violet laser ablation microprobe $^{40}Ar/^{39}Ar$ technique. Contributions to Mineralogy and Petrology 121, 1–11.

Ashwal, L.D., Tucker, R.D., Zinner, E.K., 1999. Slow cooling of deep crustal granulites and Pb-loss in zircon. Geochimica et Cosmochimica Acta 63, 2839–2851.

Beck, R.A., Burbank, D.W., Sercombe, W.J., Riley, G.W., Barndt, J.K., Berry, J.R., Afzal, J., Khan, A.M., Jurgen, H., Metje, H., Cheema, A., Shafique, N.A., Lawrence, R.D., Khan, M.A., 1995. Stratigraphic evidence for an early collision between northwest India and Asia. Nature 373, 55–58.

Belousova, E.A., Griffin, W.L., O'Reilly, S.Y., Fisher, N.I., 2002. Igneous zircon: trace element composition as an indicator of source rock type. Contributions to Mineralogy and Petrology 143, 602–622.

Compston, W., Williams, I.S., Meyer, C., 1984. U–Pb geochronology of zircons from lunar breccia 73217 using a sensitive high mass-resolution ion microprobe. Journal of Geophysical Research 89B, 525–534.

Gebauer, D., 1996. A P–T–t-path for an (ultra?-) high-pressure ultramafic/mafic rock-association and its felsic country-rocks based on SHRIMP-dating of magmatic and metamorphic zircon domains. Example: Alpe Arami (Central Swiss Alps). In: Basu, A., Hart, S.R. (Eds.), Earth Processes: Reading the Isotopic Code. American Geophysical Union, pp. 309–328.

Greco, A., Martinotti, G., Papritz, K., Ramsay, J.G., Rey, R., 1989. The Himalayan crystalline rocks of the Kaghan Valley (NE-Pakistan). Eclogae geologicae Helvetiae 82 (2), 603–627.

Hermann, J., Rubatto, D., Korsakov, A., Shatsky, V., 2001. Multiple zircon growth during fast exhumation of diamondiferous, deeply subducted continental crust (Kokchetav Massif, Kazakhstan). Contributions to Mineralogy and Petrology 141, 66–82.

Honegger, K., Dietrich, V., Frank, W., Gansser, A., Thöni, M., Trommsdorf, V., 1982. Magmatism and metamorphism in the Ladakh Himalaya (the Indus-Tsangpo suture zone). Earth and Planetary Science Letters 60, 253–292.

Hoskin, P.W.O., Black, L.P., 2000. Metamorphic zircon formation by solid-state recrystallization of protolith igneous zircon. Journal of Metamorphic Geology 18, 423–439.

Kaneko, Y., Katayama, I., Yamamoto, H., Misawa, K., Ishikawa, M., Rehman, H.U., Kausar, A.B., Shiraishi, K., 2003. Timing of Himalayan ultrahigh-pressure metamorphism: sinking rate and subduction angle of the Indian continental crust beneath Asia. Journal of Metamorphic Geology 21, 589–599.

Klootwijk, C.T., Gee, J.S., Pierce, J.W., Smith, G.M., McFadden, P.L., 1992. An early India–Asia contact: paleomagnetic constraints from Ninetyeast Ridge, ODP Leg 121. Geology 20, 395–398.

Krogh, T.E., 1973. A low-contamination method for hydrothermal decomposition of zircon and extraction of U and Pb for isotopic age determination. Geochimica et Cosmochimica Acta 37, 485–494.

Liati, A., Gebauer, D., 1999. Constraining the prograde and retrograde P–T–t path of Eocene HP rocks by SHRIMP dating different zircon domains: inferred rates of heating, burial, cooling and exhumation for central Rhodope, northern Greece. Contributions to Mineralogy and Petrology 135, 340–354.

Liu, D., Ping Jian, P., Kröner, A., Xu, S., 2006. Dating of prograde metamorphic events deciphered from episodic zircon growth in rocks of the Dabie-Sulu UHP complex, China. Earth and Planetary Science Letters 250, 650–666.

Ludwig, K.R., 2009. Isoplot 3.6, A Geochronological Toolkit for Microsoft Excel, Berkeley Geochronology Center Special Publication No. 4, Berkeley, CA, USA (Revised 08.04.08).

O'Brien, P.J., Zotov, N., Law, R., Khan, M.A., Jan, M.Q., 2001. Coesite in Himalayan eclogite and implications for models of India–Asia collision. Geology 29, 435–438.

Parrish, R.R., Krogh, T.E., 1987. Synthesis and purification of ^{205}Pb for U–Pb geochronology. Chemical Geology 66, 103–110.

Parrish, R.R., Gough, S.J., Searle, M.P., Waters, D.J., 2006. Plate velocity exhumation of ultrahigh-pressure eclogites in the Pakistan Himalaya. Geology 34, 989–992.

Patriat, P., Achache, J., 1984. India–Eurasia collision chronology has implications for crustal shortening and driving mechanism of plates. Nature 311, 615–621.

Pidgeon, R.T., 1992. Recrystallization of oscillatory zoned zircon: some geochronological and petrological implications. Contributions to Mineralogy and Petrology 110, 463–472.

Pognante, U., Spencer, D.A., 1991. First record of eclogites from the High Himalayan belt, Kaghan Valley (northern Pakistan). European Journal of Mineralogy 3, 613–618.

Rehman, H.U., Yamamoto, H., Kaneko, Y., Kausar, A.B., Murata, M., Ozawa, H., 2007. Thermobaric Structure of the Himalayan Metamorphic Belt in Kaghan Valley, Pakistan. Journal of Asian Earth Sciences 29, 390–406.

Rehman, H.U., Yamamoto, H., Khalil, M.A.K., Nakamura, E., Zafar, M., Khan, T., 2008. Metamorphic history and tectonic evolution of the Himalayan UHP eclogites in

Kaghan Valley, Pakistan. Journal of Mineralogical and Petrological Sciences 103, 242–254.
Rehman, H.U., Seno, T., Yamamoto, H., Khan, T., 2011. Timing of collision of Kohistan-Ladakh arc with India and Asia: debate. Island Arc 20, 308–328.
Rehman, H.U., Yamamoto, H., Kobayashi, K., Nakamura, E., Tsujimori, T., Ota, T., Kaneko, Y., Khan, T., 2012. Sm-Nd and Lu-Hf isotope geochemistry of the Himalayan high- and ultrahigh-pressure eclogites, Kaghan Valley, Pakistan. In: Panagiotaras, D. (Ed.), Geochemistry-Earth's System Processes. Inteck, Rijeka, Croatia, pp. 105–126.
Rubatto, D., 2002. Zircon trace element geochemistry: partitioning with garnet and the link between U–Pb ages and metamorphism. Chemical Geology 184, 123–138.
Rubatto, D., Gebauer, D., Fanning, M., 1998. Jurassic formation and Eocene subduction of the Zermatt-Saas-Fee ophiolites: implications for the geodynamic evolution of the Central and Western Alps. Contributions to Mineralogy and Petrology 132, 269–287.
Rubatto, D., Gebauer, D., Compagnoni, R., 1999. Dating of eclogite facies zircons: the age of Alpine metamorphism in the Sesia-Lanzo Zone (Western Alps). Earth and Planetary Science Letters 167, 141–158.
Rubatto, D., Hermann, J., 2003. Zircon formation during fluid circulation in eclogites (Monviso, Western Alps): implications for Zr and Hf budget in subduction zones. Geochimica et Cosmochimica Acta 67, 2173–2187.
Searle, M.P., Khan, M.A., Fraser, J.E., Gough, S.J., Jan, M.Q., 1999. The tectonic evolution of the Kohistan–Karakoram collision belt along the Karakoram highway transect, north Pakistan. Tectonics 18, 929–949.
Spencer, D.A., Tonarini, S., Pognante, U., 1995. Geochemical and Sr–Nd isotopic characterisation of Higher Himalayan eclogites (and associated metabasites). European Journal of Mineralogy 7, 89–102.
Spencer, D.A., Gebauer, D., 1996. SHRIMP Evidence for a Permian Protolith Age and a 44 Ma Metamorphic Age for the Himalayan Eclogites (Upper Kaghan, Pakistan): Implication for the Subduction of the Tethys and the Subdivision Terminology of the NW Himalaya: Himalayan–Karakoram–Tibet Workshop, 11th, Flagstaff, Arizona, USA, Abstract Volume, pp. 147–150.
Tahirkheli, R.A.K., 1979. Geology of Kohistan and adjoining area Eurasian and Indo-Pakistan continents, Pakistan. Geological Bulletin University of Peshawar 15 (Special Issue), 1–51.
Tonarini, S., Villa, I.M., Oberli, F., Meier, M., Spencer, D.A., Pognante, U., Ramsay, J.G., 1993. Eocene age of eclogite metamorphism in Pakistan Himalaya: implications for India–Eurasia collision. Terra Nova 5, 13–20.
Treloar, P.J., Williams, M.P., Coward, M.P., 1989. Metamorphism and crustal stacking in the North Indian Plate, north Pakistan. Tectonophysics 165, 167–184.
Treloar, P.J., O'Brien, P.J., Parrish, R.R., Khan, M.A., 2003. Exhumation of Early tertiary, coesite-bearing eclogites from the Pakistan Himalaya. Journal of Geological Society, London 160, 367–376.
Wasserburg, G.J., Papanastassiou, D.A., Nenow, E.V., Baumann, C.A., 1969. A programmable magnetic field mass spectrometer with on-line data processing. Reviews of Scientific Instruments 40, 288–295.
Whitehouse, M.J., Kamber, B.S., 2003. A rare earth element study of complex zircons from early Archaean Amîtsoq gneisses, Godthåbsfjord, south-west Greenland. Precambrian Research 126, 363–377.
Wilke, F.D.H., O' Brien, P.J., Altenberger, U., Konrad-Schmolke, M., Khan, M.A., 2010a. Multi-stage history in different eclogite types from the Pakistan Himalaya and implications for exhumation processes. Lithos 114, 70–85.
Wilke, F.D.H., O' Brien, P.J., Gerdes, A., Timmerman, M.J., Sudo, M., Khan, M.A., 2010b. The multistage exhumation history of the Kaghan Valley UHP series, NW Himalaya, Pakistan from U–Pb and $^{40}Ar/^{39}Ar$ ages. European Journal of Mineralogy 22, 703–719.
Zheng, Y.F., Zhao, Z.F., Wu, Y.B., Zhang, S.B., Liu, X., Wu, F.Y., 2006. Zircon U–Pb age, Hf and O isotope constraints on protolith origin of ultrahigh-pressure eclogite and gneiss in the Dabie orogen. Chemical Geology 231, 135–158.